

1 A three-dimensional eddy census of a high-resolution 2 global ocean simulation

Mark R. Petersen,¹ Sean J. Williams,^{1,2} Mathew E. Maltrud,¹ Matthew W.
Hecht,¹ Bernd Hamann,²

Bernd Hamann, Institute for Data Analysis and Visualization, Department of Computer Science, University of California, Davis CA 95616, USA.

Matthew W. Hecht, Los Alamos National Laboratory, Los Alamos, NM, 87545, USA.

Mathew E. Maltrud, Los Alamos National Laboratory, Los Alamos, NM, 87545, USA.

Mark R. Petersen, Los Alamos National Laboratory, MS B296, Los Alamos, NM, 87545, USA.
(mpetersen@lanl.gov)

Sean J. Williams, Los Alamos National Laboratory, Los Alamos, NM, 87545, USA.

¹Los Alamos National Laboratory, Los Alamos, NM, USA.

²Institute for Data Analysis and Visualization, Department of Computer Science, University of California, Davis, CA, USA.

3 **Abstract.** A three-dimensional eddy census data set was obtained from
4 a global ocean simulation with one-tenth degree resolution and a duration
5 of seven years. The census includes 6.7 million eddies in daily data, which
6 comprise 152 thousand eddies tracked over their lifetimes, using a minimum
7 lifetime cut-off of 28 days. Variables of interest include eddy diameter, thick-
8 ness (vertical extent), minimum and maximum depth, location, rotational
9 direction, lifetime, and translational speed. Distributions of these traits show
10 a predominance of small, thin, short-lived, and slow eddies. Still, a signifi-
11 cant number of eddies possess traits at the opposite extreme; thousands of
12 eddies larger than 200km in diameter appeared in daily data each year. A
13 tracking algorithm found hundreds of eddies with lifetimes longer than 200
14 days. A third of the eddies are at least 1000m tall, and many penetrate the
15 full depth of the water column. The Antarctic Circumpolar Current contains
16 the thickest and highest density of eddies. Thick eddies are also common in
17 the Gulf Stream, Kuroshio Current, and Agulhas ring pathway. The great
18 majority of eddies extend all the way to the surface, confirming that eddy
19 censuses from surface observations are a good proxy for the full-depth ocean.
20 Correlations between variables show that larger-diameter eddies tend to be
21 thicker and longer-lived than small eddies.

1. Introduction

22 How deep are ocean eddies? Do they look more like thin disks or tall columns? Do
23 eddies with large surface extents tend to be deeper as well? How many eddies are com-
24 pletely hidden below the surface? These questions are difficult to answer with current
25 observational data. Detailed eddy characteristics are available from satellite altimetry
26 [*Chelton et al.*, 2011], but provide no information about depth. Shipboard observations
27 provide some hints, but are limited to two-dimensional sections and are often shallow in
28 depth [*Timmermans et al.*, 2008; *Nishino et al.*, 2011; *Lilly and Rhines*, 2002]. Ocean
29 floats are an important tool to collect subsurface data and have begun to fill in gaps in
30 recent years, but only provide a few profiles for each eddy [*Chaigneau et al.*, 2011].

31 Numerical simulations of the ocean provide full three-dimensional velocity and tracer
32 fields that lend themselves to automated eddy census and tracking algorithms. A few
33 studies have used regional ocean simulations to investigate eddy characteristics in a par-
34 ticular area. *Doglioli et al.* [2007] tracked the three-dimensional structure of Agulhas
35 rings in an ocean simulation in order to compute transport based on the discrete eddy
36 volume. *Colas et al.* [2011] computed composite vorticity, temperature anomaly, and
37 salinity anomaly structures for cyclones and anticyclones as part of a larger study on trans-
38 port in the Peru-Chile current system. They show a three-dimensional structure where
39 maximum anomalies occur within the eddies at 100–300m depth.

40 *Dong et al.* [2012] developed a three-dimensional eddy data set of the Southern Califor-
41 nia Bight region (SCB), which provided eddy characteristics at nine vertical levels down
42 to 400m depth. They find that of the eddies that appear at the surface, less than 20%

43 reach to 50m and less than 5% extend to 100m depth (their Figure 16). Looking from
44 the bottom up, a similar tendency is seen: of the eddies that exist at 400m, only 15%
45 extend up to 250m. This data suggests that the great majority of eddies in the SCB are
46 not tall columns, but rather thin disks that are vertically isolated, both at the surface
47 and at greater depths. The lifetime and size of eddies did not vary much with depth in
48 that study, and the majority of eddies that extend from the surface to deeper levels are
49 cyclonic.

50 Eddy surveys conducted with drifters and floats typically provide information about the
51 number of loops observed and the sign of vorticity of these loops, in order to characterize a
52 region's eddy population [*Griffa et al.*, 2008; *Shoosmith et al.*, 2005; *Prater*, 2002; *Paillet*
53 *et al.*, 2002]. However, it is difficult to quantify the horizontal and vertical extents of eddies
54 with this sparse Lagrangian data. Recently, *Chaigneau et al.* [2011] demonstrated a more
55 comprehensive approach by combining Argo float profiles and satellite altimetry data to
56 analyze the vertical and horizontal structure of mesoscale eddies in the eastern South
57 Pacific Ocean. Significant differences were found between cold-core cyclonic eddies and
58 warm-core anticyclonic eddies. Composite averages of nearly 1000 Argo profiles within
59 eddies show that cyclonic eddies are shallower, with an average vertical extent of trapped
60 fluid extending to a depth of 240m versus 530m for anticyclonic eddies. The vertical
61 structure of temperature, salinity, and density anomalies are detailed for these composite
62 eddies, which allows the authors to compute heat, salt, and volume transport due to
63 eddies. Similarly, *Souza et al.* [2011a] combined float and satellite data to estimate heat
64 fluxes and transport by Agulhas rings.

65 The characterization of ocean eddies is the first step towards understanding their effects
66 in the transport of heat, salt, chemical species, and organisms. The time variability of
67 ocean currents is several times larger than the mean flow, as measured by eddy kinetic
68 energy versus mean kinetic energy in drifter observations and high resolution global models
69 [*Thoppil et al.*, 2011]. Despite the name, eddy kinetic energy is a measure of any time-
70 varying part of the velocity field, including discrete eddies as well as meandering jets
71 and waves. Discrete eddies have been shown to play a major role in observed heat and
72 salt transport [*Roemmich and Gilson*, 2001; *Chaigneau et al.*, 2011] and water mass and
73 momentum transport in model studies [*Doglioli et al.*, 2007]. Discrete eddies account
74 for 60% of the eddy kinetic energy in strongly eddying currents such as the Antarctic
75 Circumpolar Current (ACC) and western boundary currents [*Chelton et al.*, 2011].

76 Observational studies have shown that discrete eddies can have a large impact on bio-
77 logical productivity [*Everett et al.*, 2011; *Benitez-Nelson et al.*, 2007]. *Nishino et al.* [2011]
78 measured increased ammonia concentrations in a warm-core eddy that originated on the
79 shelf and moved to the Canada Basin. They suggest that the eddy was responsible for
80 sustaining 30% higher concentration of picophytoplankton biomass than that of the sur-
81 rounding waters. *Falkowski et al.* [1991] reported an increase in total primary production
82 of 20% due to eddy pumping in the tropical Pacific. Eddy-driven slumping of the basin-
83 scale north-south density gradient has been observed to cause a springtime phytoplankton
84 bloom 20-30 days earlier than would occur by warming alone [*Mahadevan et al.*, 2012].

85 How deep do the effects of eddies extend? *Adams et al.* [2011] found correlations be-
86 tween surface and deep velocities of mesoscale eddies in observations and model studies
87 of the northern East Pacific Rise. These deep-reaching eddies transport hydrothermal

88 vent efflux and vent larvae away from the Rise, and provide a mechanism for dispersing
89 propagules (plant spores) hundreds of kilometers between isolated and ephemeral commu-
90 nities. Acoustic measurements show that anticyclonic eddies shape the distribution and
91 density of marine life from the surface to depths of hundreds of meters [*Godø et al.*, 2012].

92 The purpose of this paper is to characterize eddies of the global ocean, in particular
93 properties involving depth that are somewhat sparse in observational studies. To our
94 knowledge, this is the first such eddy census of a global ocean simulation. Past work
95 on vertical eddy structure is limited to regional domains on continental shelves [*Doglioli*
96 *et al.*, 2007; *Colas et al.*, 2011; *Dong et al.*, 2012]. The paper is organized as follows: we
97 first describe the ocean model and numerical simulation (section 2) and eddy identifica-
98 tion method (section 3), followed by a description of eddy characteristics (section 4) and
99 conclusions.

2. Numerical Simulation

100 The eddy census was conducted using velocity data from seven years of a longer simu-
101 lation of POP (Parallel Ocean Program <http://climate.lanl.gov/Models>), developed and
102 maintained at Los Alamos National Laboratory [*Smith et al.*, 1992]. POP is the ocean
103 component of the Community Earth System Model (CESM, co-sponsored by the Depart-
104 ment of Energy and the National Science Foundation), which is used to study past, present
105 and future climate [*Meehl and coauthors*, 2006]. CESM simulations provide data for the
106 Intergovernmental Panel on Climate Change (IPCC) Working Group-I publications on
107 “The Physical Science Basis” for climate change [*IPCC*, 2007].

108 POP is a publicly available, z-level, hydrostatic, Boussinesq primitive equation ocean
109 model that allows for generalized orthogonal horizontal grids. In order to simulate an

110 actively eddying ocean, the particular configuration used for this study has horizontal
111 resolution of $1/10^\circ$ at the equator. The Southern Hemisphere is a standard Mercator
112 grid, while the Northern Hemisphere has two poles to avoid singularity and to provide
113 more uniform grid spacing in the Arctic, resulting in grid cell spacing ranging from 3km at
114 high latitudes to 11km at the equator. The model contains 42 fixed vertical levels ranging
115 in thickness from 10m at the surface to 250m at depth, with partial bottom cells [*Adcroft*
116 *et al.*, 1997] employed to provide a more accurate depiction of the bathymetry. Other
117 features include an implicit free surface [*Dukowicz and Smith*, 1994], vertical diffusion
118 using KPP [*Large et al.*, 1994], and biharmonic momentum and tracer diffusion. The ocean
119 is forced by monthly surface wind stress, heat fluxes, and fresh water fluxes calculated
120 from the “normal year” of the CORE data set [*Griffies et al.*, 2009], and has no explicit
121 sea ice model. Further details and references can be found in *Maltrud et al.* [2010].

3. The R^2 method of eddy identification

3.1. Motivation

122 A number of methods are available to identify eddies: sea surface height anomalies
123 above a particular threshold [*Fang and Morrow*, 2003; *Chaigneau and Pizarro*, 2005]; the
124 value of the Okubo-Weiss parameter based on velocity fields [*Isern-Fontanet et al.*, 2003];
125 and more sophisticated algorithms that combine these with a set of additional criteria
126 [*Chelton et al.*, 2011]. Other methods search for reversals in velocity sign [*Nencioli et al.*,
127 2010], or for streamlines with circular or closed geometry, like the curvature center method
128 [*Leeuw and Post*, 1995], and the winding-angle method [*Sadarjoen and Post*, 2000].

The most widely used methods are based on the Okubo-Weiss (OW) parameter W , a measure of strain versus vorticity [Isern-Fontanet et al., 2006]:

$$W = S^2 - \omega^2 \tag{1}$$

$$= s_n^2 + s_s^2 - \omega^2 \tag{2}$$

where $\omega = u_{2,1} - u_{1,2}$ is the vertical component of the relative vorticity and S , the horizontal strain, is composed of a normal component $s_n = u_{1,1} - u_{2,2}$ and a shear component $s_s = u_{1,2} + u_{2,1}$. Here $u_{i,j}$ are the components of the velocity gradient tensor. Ideally, OW contours can be used to identify vortices because OW is negative in the inner vortex core, where the flow is vorticity-dominated, positive in the strain cells surrounding the core, and small in magnitude for the remaining background flow (Figure 1). This is certainly true for idealized, periodic flows [Petersen et al., 2006], but in global ocean simulations with boundaries and realistic forcing, there are also large negative OW values along meanders of strong currents and land boundaries (Figure 2a).

A threshold of $W/\sigma_W \leq -0.2$ is typically chosen to identify the eddy edge [Isern-Fontanet et al., 2006; Henson and Thomas, 2008; Xiu et al., 2010; Petersen et al., 2006]. Here σ_W is the standard deviation of W over the region of interest, e.g. the global ocean domain in this study. However, eddy identification is sensitive to the value of σ_W and the threshold chosen. Because σ_W varies substantially over different regions of the ocean, it is not clear how to choose this value over the whole globe for this study.

For these reasons, we decided to perform our global eddy census based on the R^2 method presented in Williams et al. [2011b], which judges the fitness of a vortex based on similarity of characteristics with an idealized Gaussian vortex. Such a vortex has a Gaussian vorticity distribution in the radial direction, and has been used as a model for

148 oceanic eddies in both analytic and observational studies [*Dewar and Killworth, 1995;*
 149 *Riser et al., 1986*].

3.2. The R^2 method

The R^2 method is as follows. For each vortex identified in a W field, the algorithm begins at the minimum W value and computes the area (or volume) added with small increments of W . For a Gaussian vortex, this relationship is nearly linear in the vortex core, and then drops off dramatically at the vortex edge. Thus a simple linear regression may be used to judge how well an eddy conforms to this characteristic of a Gaussian vortex. For each vortex, at each increment of W , one computes the measure of the coefficient of determination,

$$R^2 = 1 - \frac{\sum_{i=1}^N (a_i - f_i)^2}{\sum_{i=1}^N (a_i - \bar{a})^2} \quad (3)$$

150 where a_i is the area encompassed by the W contour, $f = C_1 + C_2W$ is the best-fit line to
 151 area versus W , f_i is the value of that function for a particular W_i , $\bar{a} = \sum_{i=1}^N a_i/N$, and i
 152 increments through increasing values of W . The R^2 value describes how well a line fits the
 153 relationship between $a_1 \dots a_N$ and $W_1 \dots W_n$; a value of one indicates a perfect linear fit.
 154 In the R^2 method a confidence threshold is chosen for the full domain. For well-formed
 155 eddies, the R^2 value is above 95% within the eddy core, and then drops off outside the eddy
 156 as the area versus W fit becomes poor. For eddies that are less Gaussian-like, the R^2 value
 157 may only reach 75% or 80%. Thus in the R^2 method one chooses a confidence threshold
 158 of the fit to a Gaussian vortex, rather than a particular OW threshold or normalization.

159 In our problem of the characterization of eddies in oceanic flow, the extension of the
 160 R^2 method to the third dimension is straightforward, as the area in (3) may be replaced

161 with volume, and the rest of the algorithm remains the same. OW is computed for the
 162 full three-dimensional (3D) horizontal velocity field, i.e. at every model level. The OW
 163 computation uses horizontal velocities only, as they are several orders of magnitude larger
 164 than vertical velocities in oceanic flows. The boundary of a 3D eddy is defined by an
 165 isosurface of OW. This OW value may be different for each eddy, and is computed as the
 166 value when the linear fit of OW versus volume within that OW isosurface drops below the
 167 confidence threshold. The identification of grid cells within an eddy does not depend on
 168 the choice of OW normalization (usually the standard deviation), and could be performed
 169 on an unnormalized OW field.

To see the extension from 2D to 3D with horizontal velocities, we review the description of the R^2 method for a 2D Gaussian vortex presented in *Williams et al.* [2011b, section 3], and continue to a general formulation for a 3D ocean eddy. A 2D idealized Gaussian vortex [*Kundu et al.*, 2012, section 3.5] located at $\tilde{\mathbf{x}}$ may be described by its vorticity as a function of r , the radial direction, as

$$\omega(x, y) = c_1 \exp\left(\frac{-|\mathbf{x} - \tilde{\mathbf{x}}|^2}{2c_2^2}\right), \quad (4)$$

where $\mathbf{x} = (x, y)$, c_1 and c_2 are parameters that control the maximum strength and the width of the vortex, respectively. The extension of this idealized vortex to 3D is

$$\omega(x, y, z) = c_1(z) \exp\left(\frac{-|\mathbf{x}_{2D} - \tilde{\mathbf{x}}_{2D}(z)|^2}{2c_2^2(z)}\right), \quad (5)$$

170 where ω is the vertical component of the relative vorticity. The strength c_1 , width c_2 ,
 171 and vortex center $\tilde{\mathbf{x}}_{2D}$ may now vary in the vertical, and $\mathbf{x}_{2D} = (x, y)$. These three
 172 parameters allow the idealized vortex to take on shapes such as a column, vase, or bulb,
 173 as well as include tilting or spiraling. The only constraint is that variations in $\tilde{\mathbf{x}}_{2D}$ are

174 sufficiently small so that this remains a coherent vortex in the vertical, i.e. gridcells
175 within a particular OW isosurface remain a connected set. For a rotating, stratified
176 fluid like the ocean, vertical velocities are much smaller than horizontal velocities, so this
177 idealized vortex only considers the vertical component of vorticity. From these formulas
178 for idealized Gaussian vortices, we may compute plots of OW versus volume and OW
179 versus R^2 , as shown in *Williams et al.* [2011b, Fig 4] for 2D; 3D cases produce similar
180 curves. For more complex 3D vortices, it is best to evaluate the method on realistic eddies
181 extracted from high-resolution ocean model output. Many individual eddies were tested
182 in the development of the R^2 method; for example, the R^2 linear fit is very good for
183 a well-shaped Agulhas eddy, but poor for a deformed meander [*Williams et al.*, 2011b,
184 Fig 7]. There is no pre-imposed vertical structure used in the eddy detection algorithm.
185 Rather, the 3D structure comes directly from an isosurface in the 3D Okubo-Weiss field.

186 The R^2 algorithm is described as follows [*Williams*, 2012]. After loading velocity fields,
187 the OW field is computed for the full domain on a single day. Each local minimum in
188 OW is a potential seed point for an eddy. The volume and OW value of the seed gridcell
189 are the first entry in a record of cumulative volume and increasing OW values. From the
190 seed point, the six possible nearest neighbors (specifically, those grid cells that share a
191 face with the seed cell) are evaluated and the one with minimum OW adds a new entry to
192 the cumulative volume- OW record. The algorithm proceeds by tracking “eddy cells” and
193 “neighbor cells” of this eddy. At each iteration, the neighbor cell with the minimum OW
194 value is converted from a neighbor cell to an eddy cell. The linear fit of volume versus OW
195 is evaluated after the addition of each new eddy cell, but only after a minimum OW value
196 is passed, typically -0.5. If the coefficient of determination (3) is less than the confidence

197 threshold at that point, the eddy is not counted. Otherwise, the algorithm proceeds until
198 the coefficient of determination falls below the confidence threshold, and that value of
199 OW determines the eddy boundary (i.e., all cells recorded as “eddy cells” at that point
200 are within the eddy boundary). Census information such as location, size, depth, etc, are
201 then added to the database for that eddy. Because multiple local OW minima may exist
202 in a single eddy, the algorithm checks for duplicate eddies as it proceeds. Note that this
203 algorithm treats horizontal and vertical neighbors in the same way.

204 In order to make the R^2 algorithm more accessible to the wider community, we have
205 written a well-documented Matlab version with sample data sets, included in the elec-
206 tronic supplementary material for this article. Small sub-domains of the North Atlantic,
207 Kuroshio, and Agulhas regions have been extracted from a single daily data file of hor-
208 izontal velocity, in NetCDF format. The user may specify the confidence threshold and
209 minimum OW value for the R^2 algorithm. The code produces the eddy census data and
210 plots of velocity fields, OW, eddies identified by OW, and eddies identified by the R^2
211 method. This example code was written for clarity rather than efficiency, and may be
212 speed or memory-limited for larger data sets. Efficiency notes within the code point out
213 how to make the code faster and less memory intensive.

3.3. Tracking algorithm

214 In addition to using the R^2 method for detecting eddies, a tracking algorithm was
215 employed to provide data on eddy propagation speed and lifetime. At each consecutive
216 time sample, the algorithm searches for an eddy of similar size at the expected location
217 based on the previous eddy translation velocity. For the analysis presented here, an eddy
218 is considered the same if it appears within $1.5r$ of the expected location, where r is the

219 radius of the larger eddy, and if the radii match within 70%. The radius is the equivalent
220 radius computed from the horizontal area at the depth of the eddy's minimum OW value.
221 These parameters were adjusted so that eddy tracks with smooth trajectories were long
222 and unbroken, but were found to be stringent enough that unlikely tracks with abrupt
223 changes in direction were not included. See *Williams et al.* [2011b]; *Williams* [2012] for
224 further details. Most of the results presented in this eddy census use a minimum lifetime of
225 four weeks in order to analyze eddies that could significantly influence non-local transport
226 in the global ocean.

4. Results

227 Daily averaged velocity fields were archived from a seven year run that was restarted
228 from year 75 of the simulation described in *Maltrud et al.* [2010]. The census program
229 identified eddies from each daily average and the eddy tracking algorithm was employed to
230 collect statistics over the lifetime of each eddy. Because an eddy's characteristics change
231 over its lifetime, the statistics shown in the figures include an individual data entry for
232 each eddy on each day it was observed (similar to *Dong et al.* [2012]).

4.1. Eddy location, lifetime, and speed

233 A total of 10.9 million eddies per year (30,000 per day) were identified in these daily
234 fields using the Okubo-Weiss method with a threshold of $W/\sigma_W = -0.2$, where σ_W is the
235 standard deviation over the surface of the global domain on the initial day. Using the
236 R^2 method with 90% confidence threshold reduces this by almost a factor of three to 3.9
237 million per year (10,700 per day), where most of the removed eddies are small and thin.
238 In addition, the tracking program (which followed over 152,000 eddies over seven years)

239 was used to remove all eddies with a lifetime of less than 28 days (four weeks), reducing
240 the count to 0.96 million eddies per year (2,600 per day), or about 11 times fewer than
241 Okubo-Weiss alone.

242 Not surprisingly, the number of eddies detected by the R^2 method is sensitive to the
243 confidence threshold chosen for the Gaussian fit. Considering a single year of model
244 output, the number of accepted eddies decreases from 5.8 million at 80% to 2.4 million
245 at 95%. The majority of the rejected eddies are small, with a diameter of less than 20km
246 (Fig. 3a), which increases the mean diameter as the confidence threshold changes from
247 80% to 90% (Fig. 3c). A large number of thin eddies (less than 250m thick) are removed
248 as the confidence threshold is raised, but thick eddies are removed as well, particularly
249 as the confidence threshold is increased from 90% to 95% (Fig. 3b). The mean thickness
250 decreases by about a factor of 2 at most latitudes as the confidence interval increases
251 from 80% to 95% (Fig. 3d). As a result of this sensitivity test, it was decided that a
252 90% confidence interval would be appropriate for this study, though it is unlikely that
253 any conclusions reached would be qualitatively different if a more stringent threshold was
254 used.

255 A detailed view of the eddy density can be seen by binning daily eddy locations in each
256 1° grid cell across the globe (Figures 4a, 5b). In order to assess the fidelity of the model
257 eddy count, comparisons can be made with the altimetry-derived census of *Chelton et al.*
258 [2011]. However, such a comparison must be attempted carefully since not only are the
259 sampling methods different (three dimensional R^2 versus sea surface height criterion), so
260 are the fields that they are sampling (model versus data). In addition, this seven year
261 study includes eddies with a minimum four week lifetime, and counts the number of times

262 an eddy occurred in daily data in each one degree square, per year, while *Chelton et al.*
263 [2011] has a minimum 16 week lifetime, and counts the number of eddy centroids that pass
264 through each one degree square over a 16-year period. With these differences in mind, we
265 will emphasize the geographical distribution of eddy occurrence, rather than magnitudes
266 (Figure 5).

267 The clearest differences between the model and data are the somewhat larger meridional
268 extent of regions where no eddies are found in the model in the tropical Pacific and eastern
269 tropical Atlantic, as well as the very large number of eddies found at high latitudes in
270 the model. The former is consistent with unrealistically low model SSH variability in the
271 tropics (not shown). The latter is likely due to a number of factors. For example, the
272 model has no explicit sea ice model, which allows sampling of eddies year round at high
273 latitudes. Increasing the minimum lifetime from 4 to 16 weeks substantially reduces the
274 number of high latitude eddies (not shown) but this bias remains a question for further
275 study.

276 There is also an encouraging amount of agreement to be seen in Figure 5. Regions
277 of low eddy density in the North Pacific and the eastern South Pacific have been called
278 “eddy deserts” [*Chelton et al.*, 2011] and are clearly visible in both the data and model.
279 Subtropical zonal bands with high eddy counts can be seen in all basins. In the model,
280 these bands are more sharply peaked as the eddies tend to follow similar paths from year
281 to year. This is possibly due to the fact that the model is forced with repeating monthly
282 climatology, and that the wind stress calculation does not include the contribution from
283 the surface ocean velocity. Similarities can also be seen in the the eastern basin upwelling
284 zones off the west coasts of Australia, Peru, and the United States.

285 It is interesting to note that the eddy count in the central and eastern Arctic is ex-
286 tremely sparse (Fig. 4a). Unfortunately, very few long term observations are available
287 (*e.g.*, [Timmermans *et al.*, 2008]) in the high Arctic, so it is difficult to draw conclusions
288 about the fidelity of the simulation there. It is likely that a combination of factors may
289 be causing this, such as insufficient grid resolution, strong restoring of surface tempera-
290 ture and salinity (30 day time scale) to climatological values under prescribed sea ice, or
291 unrealistic model density structure. An eddy census of higher fidelity simulations of the
292 Arctic with dynamic sea ice and higher resolution, like those in Maslowski *et al.* [2008],
293 may shed light on this question.

294 Collecting eddies into 1° latitude bins allows for a quantitative comparison of the R^2
295 method and Okubo-Weiss. The R^2 method reduces the eddy count quite uniformly at
296 mid to high latitudes (Fig. 6a), but culls somewhat more strongly in the tropics, where
297 the eddies that are removed tend to be thin and small (Fig. 6b,c).

298 Figure 7a shows a histogram of lifetimes for all eddies identified over the seven year
299 period. As noted above, 75% of eddies identified in daily averages have lifetimes of less
300 than 28 days, and were discarded from the analysis since such short-lived eddies are
301 typically not coherent structures involved in non-local transport. The longest-lived eddy
302 existed for a duration of 1143 days, nearly half the span of the full data set. This eddy
303 remains nearly still and isolated in the Gulf of St. Lawrence (green track in Figure 8)
304 with a mean thickness of 419m and mean diameter of 69km. Other eddies with lifetimes
305 greater than 550 days include three off the coast of Chile, two in the ACC, and one in the
306 north-west Pacific.

307 An image of the 5000 longest lived eddies (Figure 8) shows an abundance of eddies in the
308 ACC; these tracks appear relatively short and chaotic, and propagate in all directions. In
309 contrast, the mid-latitude eddy tracks are smoother, longer, and predominantly westward.
310 Several tracks have a looping behavior, such as two brown tracks in the mid North Atlantic.
311 The tracked Agulhas Rings are particularly long and stable, and are visible all the way to
312 South America. Because this eddy tracking routine requires similar radii to match from
313 frame to frame, an event that changes eddy characteristics, like merger or shearing in a
314 jet, will sometimes split what appears to be a single track.

315 The tracking algorithm measures the speed of eddy propagation by computing the dis-
316 tance traveled from one day to the next (Fig. 7b). The distribution follows a logarithmic
317 drop-off, with 72% of eddies slower than 10cm/s, and 93% slower than 20cm/s. This range
318 is similar to observations [*Chelton et al.*, 2011, Fig. 22]. Speeds higher than 20cm/s are
319 visible in the strong currents of the Gulf Stream, Kuroshio, equatorial jets, and the ACC
320 (Figure 4e).

321 In order to characterize the effects of eddies over their lifetimes, the average distance,
322 speed, and direction were computed using the locations of the first and last day provided by
323 the tracking algorithm (Fig. 9). The globe was separated into regions as follows: Southern
324 Ocean south of 42S; North Atlantic: 0–65N and 90W–20E; South Atlantic: 0–42S, 65–
325 20E; North Pacific: 0–65N, 100E–90W; South Pacific: 0–42S, 100E–65W; Indian: 42S–
326 30N, 20E–100E. The Southern Ocean stands out as the region with the shortest lifetime
327 distance, with most eddies traveling less than 100km. This can be seen qualitatively
328 in the images of eddy tracks (Fig. 8), and is due to the pervasively strong flows of
329 the ACC. Over most of the globe there is a strong preference for westward motion over

330 the lifetime of the eddy, as expected from Rossby wave dynamics. The Southern Ocean
331 presents an exception, where the eastward background flow may be as fast or faster than
332 the eddy's intrinsic propagation speed. Outside of the Southern Ocean, eddies in the
333 northern hemisphere travel shorter distances and slower speeds than those in the southern
334 hemisphere. Figure 8 shows more long, smooth paths between the equator and 42S, while
335 eddy tracks in the strong western boundary currents of the northern hemisphere are short
336 and chaotic.

4.2. Eddy diameter

337 Figure 4b shows a global view of the effective diameter of the identified eddies, defined
338 as $d = 2\sqrt{A/\pi}$, where A is the horizontal cross-sectional area of the eddy recorded at the
339 depth with the most negative Okubo-Weiss value. Clearly the eddy diameter is a strong
340 function of latitude, with smaller eddies near the poles and larger ones near the equator.
341 This is expected since the first baroclinic Rossby radius varies strongly with latitude (as
342 shown by the dashed line in Figure 6c), and length scales for mesoscale eddies typically
343 are linearly related to the Rossby radius but are larger [Stammer, 1997].

344 Zonal averages of eddy length scales provide another opportunity for quantitative com-
345 parison of the R^2 method with Okubo-Weiss, as well as with *Chelton et al.* [2011] (Figure
346 6c). The R^2 method removes many of the small and poorly-formed eddies identified by
347 the Okubo-Weiss method, thus increasing the average diameter, especially after filtering
348 out relatively short-lived eddies. As with the eddy density, comparisons of length scale
349 with data should focus more on shapes than magnitudes (*Chelton et al.* [2011] describe
350 four methods of computing eddy length scales in their appendix B.3, which vary by as
351 much as a factor of 3.7 in overall scale). The Pearson correlation coefficient (computed for

latitudes where observations are available (68S to 70N) and outside of the tropics) relating the zonally averaged model to data length scales (black and purple curves in Figure 6c, respectively) is 0.94; a value of 1.0 is expected if the the two curves are proportional or offset. Although the model and data agree very well, they both have a somewhat weaker dependence on latitude than the Rossby radius. Zonal averages of eddy diameter with varying confidence thresholds were computed using a single year’s data (Fig 3c). The Pearson correlation coefficient increases systematically with increasing confidence threshold: 0.901 for 80%, 0.925 for 85%, 0.941 for 90% and 0.943 for 95%. The improved fit of model data versus observation provides further evidence that a 90% confidence threshold is the appropriate choice for this study.

Evaluating eddy diameter by region (Fig. 4b), the model agrees well with the observations (*Griffa et al.* [2008, Fig. 3], *Chelton et al.* [2007, Fig. 3]) in the Gulf Stream and Kuroshio Current systems, as well as in the Mozambique channel, in the “Cape Cauldron” [*Boebel et al.*, 2003] to the west of the Cape of Good Hope, and along much of the Sub-Antarctic Front in the ACC. However, it appears that the simulations and R^2 method substantially underestimate the eddy diameter in the Agulhas Retroflexion (particularly directly south of the African continent) and the Brazil-Malvinas Confluence. The striking maximum in the South Atlantic at about $20^\circ S$ is due to a few large Agulhas eddies that have traversed the ocean quite a bit too far to the north.

4.3. Cyclonicity

The direction of eddy rotation, averaged by 1° bins, is shown in Figure 4d. In the Indian ocean, a blue cyclonic band is visible between 10S and 20S, while a red anticyclonic band appears between 20S and 30S. This is similar to Lagrangian drifter survey data [*Griffa*

374 *et al.*, 2008, Fig. 3]. The data hints at some other coherent zonal structures, but overall
375 spatial patterns are difficult to find, much like satellite observations [*Chelton et al.*, 2011,
376 Fig. 4].

377 The eddy census includes more anti-cyclonic eddies; 46% of eddies are cyclonic overall.
378 This behavior varies smoothly with diameter, with small (large) diameter eddies tending
379 to be more anticyclonic (cyclonic) (Fig. 11a). This behavior crosses over at 120km in
380 diameter, and eddies larger than 225km in diameter have a strong preference for cyclonic
381 behavior. Cyclonicity does not appear to vary with thickness in a regular way (Fig.
382 11b). To our knowledge, there are no reported observations of cyclonicity as a function of
383 diameter or thickness. *Chelton et al.* [2011] reports more cyclones than anticyclones for
384 eddies with a lifetime of less than 60 weeks, which is opposite our finding.

4.4. Origin and Termination

385 The tracking algorithm allows the identification of origin and termination locations for
386 each eddy. These were collected in 1° bins to show regions of origin and termination (not
387 shown). The geographical distribution of origin and termination are the largely same as
388 each other, and similar to daily recorded eddy locations (Fig. 4a); these are all highest
389 in the ACC, Gulf Stream, and Kuroshio Current regions. *Chelton et al.* [2011] also find
390 that origin and termination sites are common in open-ocean regions wherever propagating
391 eddies occur (their Figure 6). This is consistent with studies that show that nearly all
392 of the world ocean is baroclinically unstable [*Smith*, 2007; *Stammer*, 1998]. Plotting
393 the difference between origin and termination global distributions (not shown), coastal
394 regions have a higher number of eddy generation sites on eastern boundaries, and more
395 terminations on western boundaries, as one would expect when a majority of eddies are

396 propagating westward (Fig. 9e,f). This same pattern is evident in satellite observations
397 [*Chelton et al.*, 2011, Fig. 6]. As noted by *Dong et al.* [2012] in their regional simulations
398 of the Southern California Bight, eddy creation can be strongly influenced by topography,
399 which can also be seen in this global simulation.

4.5. Vertical Characteristics

400 One major advantage of using fully three dimensional model fields is the ability to
401 investigate the vertical characteristics of eddies. For each eddy, the R^2 method finds the
402 highest Okubo-Weiss value where the 90% confidence threshold is maintained. The three-
403 dimensional surface of this Okubo-Weiss value defines the eddy extent, so that the census
404 database includes a minimum depth, maximum depth, and thus a thickness (difference
405 between the two) for each eddy on every day. The R^2 method finds the eddy surface
406 by determining where the Okubo-Weiss value no longer fits, to a particular confidence
407 threshold, the linear relationship that would be expected with the inclusion of additional
408 volume, if the eddy's vorticity were perfectly Gaussian in its dependence on radial distance
409 from the core. There will be some vortical motion beyond the eddy's boundary surface,
410 but it is substantially weaker than within the eddy.

411 The zonally binned thickness (Figure 6b) is the greatest in the Southern Ocean, due in
412 part to a fairly uniform longitudinal distribution in the ACC as well as some very thick
413 eddies to the north and west of the Weddell Sea (Figure 4c). Thick eddies ($\sim 2000\text{m}$) are
414 also typically found in the extension regions of the major western boundary currents as
415 well as the North Brazil Current and the Gulf of Mexico.

416 As is the case for the horizontal scale, the R^2 method does not have an explicit thickness
417 criteria, but thin eddies are more strongly removed than with Okubo-Weiss alone because

418 most poorly-formed eddies are also thin. The R^2 method approximately doubles the
419 globally averaged thickness, compared to Okubo-Weiss, and restricting to eddies with a
420 minimum lifetime of four weeks further removes thin eddies (Figure 6b).

421 Overall, the majority of eddies are thin (Figure 10b). Still, there is a significant popu-
422 lation of thick eddies since the distribution shows that 40%, 16%, and 7.7% are at least
423 1000m, 2000m, and 3000m thick, respectively. In order to provide a qualitative image
424 of vertical eddy extent, a skeletonized view is provided in Figure 12, showing that some
425 eddies extend to the full column depth in the Gulf Stream, while most eddies extend to
426 the bottom in the Southern Ocean.

427 In addition to thickness, we can also locate the extents of eddies within the water
428 column. The great majority of eddies observed in the daily data extend all the way to the
429 surface (Figure 10c,d), with 97% expressed in the model’s 10m-thick uppermost threshold
430 for eddies tracked for at least four weeks, and 89% with no lifetime restriction. This does
431 not necessarily imply that the remaining eddies would be missed in observational studies
432 of SSH using satellite altimetry. Not all eddies that extend to the surface have a clear SSH
433 signature, while some eddies that do not reach the surface *can* be detected in the SSH. To
434 quantify the percentage of eddies that are missed would require correlating these results
435 with an SSH-based detection algorithm, such as *Chelton et al.* [2011], which is beyond the
436 scope of this paper.

437 The tracking program allows us to quantify vertical characteristics over the lifetime of
438 each eddy. To this end, we define “subsurface” to mean that the top of the eddy boundary
439 surface is below 100m. Figure 13 shows the percentage of days that the eddy is subsurface
440 over its lifetime. The great majority of eddies extend above 100m at least 95% of the time

441 (91% globally). One might expect that subsurface eddies remain so for the duration of
442 their lifetime. However, that is not the case. Eddies tracked over their lifetime that are
443 subsurface some days extend to the surface on other days. Figure 13 shows that many
444 eddies are subsurface 5–20% of the time, and very few are subsurface all the time.

445 Going one step further, what are the characteristics of subsurface eddies that will largely
446 be missed by satellite observations? For this purpose, we define subsurface eddies as those
447 below 100m at least 50% of their lifetime, and surface eddies as those below 100m for 5% of
448 their lifetime or less. Subsurface eddies have a much shorter lifespan than surface eddies,
449 and no subsurface eddies were found with lifetimes longer than 125 days, while surface
450 eddies often live for 200–600 days (Fig. 14). Subsurface eddies are smaller than surface
451 eddies, with 40% in the 30–40km diameter category. The thickness distribution does not
452 follow this pattern. Most subsurface eddies are 1500–3500m thick, while more than half
453 of surface eddies are less than 1000m thick.

4.6. Multivariate Distributions

454 Given the numerous properties that the eddy census provides, it is now possible to
455 look for relationships between them. For example, Figure 15 shows a two-dimensional
456 histogram of diameter and thickness. For most of the range of both diameter (50 - 150m)
457 and thickness (500 - 4500m), there is no clear correlation. That is, knowledge of an eddy's
458 diameter yields no specific information about its thickness, and vice versa. However, the
459 extremes in the distribution do show that small eddies tend to be thinner than normal and
460 very thick eddies tend to have larger diameters than normal. Quantitatively, the Pearson
461 correlation coefficient between diameter and thickness is 0.154, where 1.0 means the two
462 variables are linearly dependent, and zero implies no correlation.

463 Based on kinematic considerations, one might expect that larger eddies would tend to
464 be longer lived than smaller ones since they contain more mass and momentum, and are
465 less likely to be torn apart by background shear or when passing over deep-sea ridges. This
466 does appear to be the case here. A clear correlation exists between mean eddy diameter
467 and lifetime (stars on Figure 16a), as quantified by a Pearson correlation coefficient of
468 0.261. Similarly, fast eddies tend to be larger in diameter (stars on Figure 16b). There also
469 is a noticeable relationship between thickness and speed, showing a tendency for thinner
470 eddies to move somewhat faster. Quantitatively, however, the Pearson correlation is only
471 0.017 so this may only be relevant to speeds under about 20 cm/s.

5. Conclusions

472 Seven years of daily output from a global high resolution POP simulation has allowed us
473 to locate and characterize 6.7 million eddies using the R^2 method (*Williams et al.* [2011b])
474 and a tracking algorithm. While this work is preceded by many studies of eddies in regional
475 ocean simulations such as *Doglioli et al.* [2007]; *Nencioli et al.* [2010]; *Souza et al.* [2011b];
476 *Dong et al.* [2012]; *Doglioli et al.* [2007]; *Colas et al.* [2011] (a few of which also evaluate
477 the vertical aspects of the eddy field), we believe that this is the first systematic eddy
478 census of a three-dimensional high resolution global ocean simulation. Our goal in this
479 study is to provide statistical information on eddies throughout the global ocean, as done
480 with satellite altimetry investigations [*Chelton et al.*, 2007; *Chelton et al.*, 2011], but to
481 also describe eddy characteristics that are hidden below the surface. In addition, detailed
482 quantitative information about eddy speed and lifetime may prove useful in attempts to
483 parameterize the nonlocal effects of eddies in simulations where they are not explicitly
484 represented.

485 A significant number of eddies penetrate deep into the ocean: a third of the eddies in
486 this simulation are at least 1000m tall. Of eddies with a minimum four weeks lifetime, the
487 majority (97%) extend all of the way to the surface. Although not all of these surface-
488 expressed eddies located by the R^2 method are clearly reflected in the surface height, it is
489 very likely that satellite altimetry-based assessments of eddy size, spatial distribution, and
490 lifetime are reasonably comprehensive as estimates of eddy characteristics. The remaining
491 eddies that do not reach the surface are distributed over the full depth of the ocean, with
492 thousands deeper than 3000m. Larger-diameter eddies are likely to be thicker, longer-
493 lived, and faster than smaller-diameter eddies. Correlations between thickness and lifetime
494 or thickness and speed are weak, except that very thin eddies are fast and shorter-lived.

495 Any eddy census method is dependent on the eddy detection method, and the param-
496 eters chosen within that method. Because the R^2 method is relatively new, we include
497 a traditional Okubo-Weiss method in some plots for direct comparison. The R^2 method
498 judges the quality of an eddy based on the similarity of certain functional fits with an
499 idealized Gaussian vortex. We find that R^2 is more selective than Okubo-Weiss and pref-
500 erentially removes smaller and thinner eddies. It improves global statistics, such as mean
501 diameter versus latitude, to be more like observations and theoretical expectations. For
502 this study we have primarily used an R^2 confidence threshold of 90%, which appears to
503 mostly select well-formed, coherent, and long-lived eddies. Absolute numbers of eddies
504 counted are sensitive to choices of methods and parameters used for detection, so we have
505 included distributions and percentages throughout the paper. Choices of model settings,
506 such as diffusion coefficients and advection schemes, can also affect the number and char-
507 acteristics of simulated eddies, but quantifying sensitivity to these factors is prohibitively

508 expensive for a global eddying model. In addition, experience has shown that there is a
509 relatively narrow range of parameter space that provides smooth solutions and yet allows
510 for strongly developed mesoscale variability that compares well with observations [*Bryan*
511 *et al.*, 2007]. Thus it is unlikely that acceptable variations in the model configuration
512 would result in substantial changes to the results presented here.

513 The first priority in an ocean modeling study is to confirm that simulations are in
514 reasonable agreement with observational data, wherever that data is available. Other
515 authors have conducted comparisons of the POP ocean model at a resolution of one-tenth
516 degree with observations of volume transport, kinetic energy, and eddy kinetic energy
517 and have found good agreement [*Smith et al.*, 2000; *Bryan et al.*, 2007; *Maltrud and*
518 *McClean*, 2005]. In the eddy data presented here, a comparison of eddy count, diameter,
519 and rotational direction was made with figures in *Chelton et al.* [2011] and *Griffa et al.*
520 [2008]. General trends, such as increasing diameter towards the equator, are similar to
521 observed, but geographical distributions of eddy characteristics did not match in some
522 cases. This was complicated by the fact that satellite observations [*Chelton et al.*, 2011]
523 and drifter trajectories [*Griffa et al.*, 2008] were not always in agreement.

524 Beyond surface studies, is there a way to confirm the deeper data? Here we turn to
525 *Thoppil et al.* [2011], who found that a simulation using HYCOM at $1/12.5^\circ$ resolution,
526 is deficient in eddy kinetic energy in both the upper and abyssal ocean (depths greater
527 than 3000 m) by 21% and 24% respectively compared to surface drifting buoys and deep
528 current meters (increasing the resolution to $1/25^\circ$ alleviated the problem). Our study
529 used a $1/10^\circ$ POP simulation, but generally we can expect that ocean simulations at this

530 resolution may be underresolved for some eddy processes, and may underrepresent eddy
531 activity, perhaps by as much as 20-25%.

532 Even with this discrepancy, we can confidently conclude that eddies are a common
533 phenomenon in the deep ocean, albeit in smaller numbers than thin eddies near the
534 surface. Observational studies of eddy transport of heat and nutrients [*Roemmich and*
535 *Gilson, 2001; Chaigneau et al., 2011; Doglioli et al., 2007*] have been confined to the upper
536 ocean for practical reasons. The next step in the analysis of this simulation is to quantify
537 the impact of discrete eddies on the transport of tracers throughout the globe. Indeed,
538 high resolution ocean model output provides the unique opportunity to compute detailed
539 statistics where observations are sparse. Our team has recently developed a method to
540 compute tracer fluxes through eddy boundaries [*Williams et al., 2012*]. In future work we
541 plan to seed eddies in global simulations with passive tracers, leading to eddy transport
542 and containment statistics for various regions of the earth.

543 **Acknowledgments.** The authors thank Milena Veneziani and Wilbert Weijer for early
544 comments on the manuscript, and Neesha Regmi Schnepf for assistance with the literature
545 search on vortex identification methods. We also thank Richard Strelitz and Samantha
546 Oestricher for insightful discussions. Dudley Chelton and Michael Schlax generously gave
547 us access to their altimetry-derived eddy census data. MRP, MWH, and MEM were
548 supported by the Regional and Global Climate Modeling programs; SJW was supported by
549 the UV-CDAT project in the Climate and Earth System Modeling programs. Both of these
550 are within the Office of Biological and Environmental Research of the US Department of
551 Energy's Office of Science. We acknowledge the support of the LANL-UC Davis Materials
552 Design Institute for SJW and BH.

References

- 553 Adams, D. K., D. J. McGillicuddy, L. Zamudio, A. M. Thurnherr, X. Liang, O. Rouxel,
554 C. R. German, and L. S. Mullineaux, Surface-Generated Mesoscale Eddies Transport
555 Deep-Sea Products from Hydrothermal Vents, *Science*, *332*, 580–, 2011.
- 556 Adcroft, A., C. Hill, and J. Marshall, Representation of Topography by Shaved Cells in a
557 Height Coordinate Ocean Model, *Monthly Weather Review*, *125*, 2293, 1997.
- 558 Benitez-Nelson, C. R., et al., Mesoscale Eddies Drive Increased Silica Export in the Sub-
559 tropical Pacific Ocean, *Science*, *316*, 1017–, 2007.
- 560 Boebel, O., J. Lutjeharms, C. Schmid, W. Zenk, T. Rossby, and C. Barron, The Cape
561 Cauldron: a regime of turbulent inter-ocean exchange, *Deep Sea Research Part II:
562 Topical Studies in Oceanography*, *50*, 57–86, 2003.
- 563 Bryan, F. O., M. W. Hecht, and R. D. Smith, Resolution convergence and sensitivity
564 studies with North Atlantic circulation models. Part I: The Western Boundary Current
565 system, *Ocean Modelling*, *16*, 141–159, 2007.
- 566 Chaigneau, A., and O. Pizarro, Eddy characteristics in the eastern South Pacific, *Journal
567 of Geophysical Research (Oceans)*, *110*, 6005, 2005.
- 568 Chaigneau, A., M. Le Texier, G. Eldin, C. Grados, and O. Pizarro, Vertical structure
569 of mesoscale eddies in the eastern South Pacific Ocean: A composite analysis from
570 altimetry and Argo profiling floats, *Journal of Geophysical Research (Oceans)*, *116*,
571 11,025, 2011.
- 572 Chelton, D. B., M. G. Schlax, R. M. Samelson, and R. A. de Szoeke, Global observations
573 of large oceanic eddies, *Geophysical Research Letters*, *34*, 5, 2007.

- 574 Chelton, D. B., M. G. Schlax, and R. M. Samelson, Global observations of nonlinear
575 mesoscale eddies, *Progress in Oceanography*, *91*, 167–216, 2011.
- 576 Colas, F., J. C. McWilliams, X. Capet, and J. Kurian, Heat balance and eddies in the
577 Peru-Chile current system, *Climate Dynamics*, p. 582, 2011.
- 578 Dewar, W. K., and P. D. Killworth, On the Stability of Oceanic Rings, *Journal of Physical*
579 *Oceanography*, *25*, 1467–1487, 1995.
- 580 Doglioli, A. M., B. Blanke, S. Speich, and G. Lapeyre, Tracking coherent structures in a
581 regional ocean model with wavelet analysis: Application to Cape Basin eddies, *Journal*
582 *of Geophysical Research (Oceans)*, *112*, 5043, 2007.
- 583 Dong, C., X. Lin, Y. Liu, F. Nencioli, Y. Chao, Y. Guan, D. Chen, T. Dickey, and J. C.
584 McWilliams, Three-dimensional oceanic eddy analysis in the Southern California Bight
585 from a numerical product, *Journal of Geophysical Research (Oceans)*, *117*, 0, 2012.
- 586 Dukowicz, J. K., and R. D. Smith, Implicit free-surface method for the Bryan-Cox-Semtner
587 ocean model, *J. Geophys. Res.*, *99*, 7991–8014, 1994.
- 588 Everett, J. D., M. E. Baird, and I. M. Suthers, Three-dimensional structure of a swarm
589 of the salp *Thalia democratica* within a cold-core eddy off southeast Australia, *Journal*
590 *of Geophysical Research (Oceans)*, *116*, 12,046, 2011.
- 591 Falkowski, P. G., D. Ziemann, Z. Kolber, and P. K. Bienfang, Role of eddy pumping in
592 enhancing primary production in the ocean, *Nature*, *352*, 55–58, 1991.
- 593 Fang, F., and R. Morrow, Evolution, movement and decay of warm-core Leeuwin Current
594 eddies, *Deep Sea Research Part II: Topical Studies in Oceanography*, *50*, 2245–2261,
595 2003.

- 596 Godø, O. R., A. Samuelsen, G. J. Macaulay, R. Patel, S. S. Hjøllo, J. Horne, S. Kaartvedt,
597 and J. A. Johannessen, Mesoscale eddies are oases for higher trophic marine life, *PLoS*
598 *ONE*, 7, e30,161, 2012.
- 599 Griffa, A., R. Lumpkin, and M. Veneziani, Cyclonic and anticyclonic motion in the upper
600 ocean, *Geophys. Res. Lett.*, 35, 1608, 2008.
- 601 Griffies, S. M., et al., Coordinated Ocean-ice Reference Experiments (COREs), *Ocean*
602 *Modelling*, 26, 1–46, 2009.
- 603 Henson, S. A., and A. C. Thomas, A census of oceanic anticyclonic eddies in the Gulf
604 of Alaska, *Deep Sea Research Part I: Oceanographic Research Papers*, 55, 163 – 176,
605 2008.
- 606 IPCC, *Climate Change 2007: The Physical Science Basis. Contribution of Working Group*
607 *I to the Fourth Assessment Report of the Intergovernmental Panel on Climate Change*,
608 Cambridge University Press, 2007.
- 609 Isern-Fontanet, J., E. Garca-Ladona, and J. Font, Identification of marine eddies from
610 altimetric maps., *Journal of Atmospheric & Oceanic Technology*, 20, 772, 2003.
- 611 Isern-Fontanet, J., E. Garca-Ladona, J. Font, and A. Garca-Olivares, Non-gaussian veloc-
612 ity probability density functions: An altimetric perspective of the mediterranean sea.,
613 *J. Phys. Oceanogr.*, 36, 2153 – 2164, 2006.
- 614 Kundu, P. K., I. M. Cohen, and D. R. Dowling, *Fluid Mechanics*, fifth ed., Academic
615 Press, 2012.
- 616 Large, W. G., J. C. McWilliams, and S. C. Doney, Oceanic vertical mixing: a review and
617 a model with a nonlocal boundary layer parameterization, *Rev. Geophys.*, 32, 363–404,
618 1994.

- 619 Leeuw, and Post, *A Statistical View on Vector Fields*, Visualization in Scientific Comput-
620 ing, Springer-Verlag, 1995.
- 621 Lilly, J. M., and P. B. Rhines, Coherent Eddies in the Labrador Sea Observed from a
622 Mooring, *Journal of Physical Oceanography*, *32*, 585–598, 2002.
- 623 Mahadevan, A., E. D’Asaro, C. Lee, and M. J. Perry, Eddy-driven stratification initiates
624 north atlantic spring phytoplankton blooms, *Science*, *337*, 54–58, 2012.
- 625 Maltrud, M., F. Bryan, and S. Peacock, Boundary impulse response functions in a century-
626 long eddying global ocean simulation, *Environmental Fluid Mechanics*, *10*, 275–295,
627 2010, 10.1007/s10652-009-9154-3.
- 628 Maltrud, M. E., and J. L. McClean, An eddy resolving global $1/10^\circ$ ocean simulation,
629 *Ocean Modelling*, *8*, 31–54, 2005.
- 630 Maslowski, W., J. L. C. Kinney, D. C. Marble, and J. Jakacki, Towards eddy-resolving
631 models of the Arctic ocean, in *Ocean Modeling in an Eddying Regime*, edited by
632 M. Hecht and H. Hasumi, no. 177 in Geophysical Monograph Series, pp. 241–264, Amer-
633 ican Geophysical Union, Washington, D.C., 2008.
- 634 Meehl, G. A., and coauthors, Climate change projections for the twenty-first century and
635 climate change commitment in the CCSM3, *J. Climate*, *19*, 2597–2616, 2006.
- 636 Nencioli, F., C. Dong, T. Dickey, L. Washburn, and J. C. McWilliams, A vector geometry-
637 based eddy detection algorithm and its application to a high-resolution numerical model
638 product and high-frequency radar surface velocities in the southern california bight,
639 *Journal of Atmospheric and Oceanic Technology*, *27*, 564–579, 2010.
- 640 Nishino, S., M. Itoh, Y. Kawaguchi, T. Kikuchi, and M. Aoyama, Impact of an unusually
641 large warm-core eddy on distributions of nutrients and phytoplankton in the southwest-

- 642 ern Canada Basin during late summer/early fall 2010, *Geophys. Res. Lett.*, *38*, 16,602,
643 2011.
- 644 Paillet, J., B. Le Cann, X. Carton, Y. Morel, and A. Serpette, Dynamics and Evolution
645 of a Northern Meddy, *Journal of Physical Oceanography*, *32*, 55–79, 2002.
- 646 Petersen, M. R., K. Julien, and J. B. Weiss, Vortex cores, strain cells, and filaments in
647 quasigeostrophic turbulence, *Physics of Fluids*, *18*, 026,601–+, 2006.
- 648 Prater, M. D., Eddies in the Labrador Sea as Observed by Profiling RAFOS Floats and
649 Remote Sensing, *Journal of Physical Oceanography*, *32*, 411–427, 2002.
- 650 Riser, S. C., W. B. Owens, H. T. Rossby, and C. C. Ebbesmeyer, The Structure, Dynamics,
651 and Origin of a Small-Scale Lens of Water in the Western North Atlantic Thermocline,
652 *Journal of Physical Oceanography*, *16*, 572–590, 1986.
- 653 Roemmich, D., and J. Gilson, Eddy Transport of Heat and Thermocline Waters in the
654 North Pacific: A Key to Interannual/Decadal Climate Variability?, *Journal of Physical*
655 *Oceanography*, *31*, 675–688, 2001.
- 656 Sadarjoen, I. A., and F. H. Post, Detection, quantification, and tracking of vortices using
657 streamline geometry, *Computers & Graphics*, *24*, 333 – 341, 2000.
- 658 Shoosmith, D. R., P. L. Richardson, A. S. Bower, and H. T. Rossby, Discrete eddies in
659 the northern North Atlantic as observed by looping RAFOS floats, *Deep Sea Research*
660 *Part II: Topical Studies in Oceanography*, *52*, 627–650, 2005.
- 661 Smith, K. S., The geography of linear baroclinic instability in Earth’s oceans, *J. Mar.*
662 *Res.*, *65*, 655–683, 2007.
- 663 Smith, R. D., J. K. Dukowicz, and R. C. Malone, Parallel ocean general circulation
664 modeling, *Physica D*, *60*, 38–61, 1992.

- 665 Smith, R. D., M. E. Maltrud, F. O. Bryan, and M. W. Hecht, Numerical simulation of
666 the North Atlantic Ocean at $1/10^\circ$, *J. Phys. Oceanogr.*, *30*, 1532–1561, 2000.
- 667 Souza, J. M. A. C., C. de Boyer Montégut, C. Cabanes, and P. Klein, Estimation of the
668 Agulhas ring impacts on meridional heat fluxes and transport using ARGO floats and
669 satellite data, *Geophys. Res. Lett.*, *38*, 21,602, 2011a.
- 670 Souza, J. M. A. C., C. de Boyer Montégut, and P. Y. Le Traon, Comparison between
671 three implementations of automatic identification algorithms for the quantification and
672 characterization of mesoscale eddies in the South Atlantic Ocean, *Ocean Science*, *7*,
673 317–334, 2011b.
- 674 Stammer, D., Global Characteristics of Ocean Variability Estimated from Regional
675 TOPEX/POSEIDON Altimeter Measurements, *Journal of Physical Oceanography*, *27*,
676 1743–1769, 1997.
- 677 Stammer, D., On Eddy Characteristics, Eddy Transports, and Mean Flow Properties,
678 *Journal of Physical Oceanography*, *28*, 727–739, 1998.
- 679 Thoppil, P. G., J. G. Richman, and P. J. Hogan, Energetics of a global ocean circulation
680 model compared to observations, *Geophys. Res. Lett.*, *38*, 15,607, 2011.
- 681 Timmermans, M.-L., J. Toole, A. Proshutinsky, R. Krishfield, and A. Plueddemann, Ed-
682 dies in the Canada Basin, Arctic Ocean, Observed from Ice-Tethered Profilers, *Journal*
683 *of Physical Oceanography*, *38*, 133, 2008.
- 684 Williams, S., M. Hecht, M. Petersen, R. Strelitz, M. Maltrud, J. Ahrens, M. Hlawitschka,
685 and B. Hamann, Visualization and analysis of eddies in a global ocean simulation,
686 *Computer Graphics Forum*, *30*, 991–1000, 2011a.

- 687 Williams, S., M. Petersen, P.-T. Bremer, M. Hecht, V. Pascucci, J. Ahrens, M. Hlaw-
688 itschka, and B. Hamann, Adaptive extraction and quantification of geophysical vortices,
689 *IEEE Transactions on Visualization and Computer Graphics*, *17*, 2088–2095, 2011b.
- 690 Williams, S., M. Petersen, M. Hecht, M. Maltrud, J. Patchett, J. Ahrens, , and
691 B. Hamann, Interface exchange as an indicator for eddy heat transport, *Computer*
692 *Graphics Forum*, *31*, 1125–1134, 2012.
- 693 Williams, S. J., Identification and quantification of mesoscale eddies in a global ocean
694 simulation, Ph.D. thesis, University of California, Davis, 2012.
- 695 Xiu, P., F. Chai, L. Shi, H. Xue, and Y. Chao, A census of eddy activities in the South
696 China Sea during 1993-2007, *Journal of Geophysical Research*, *115*, 564–579, 2010.

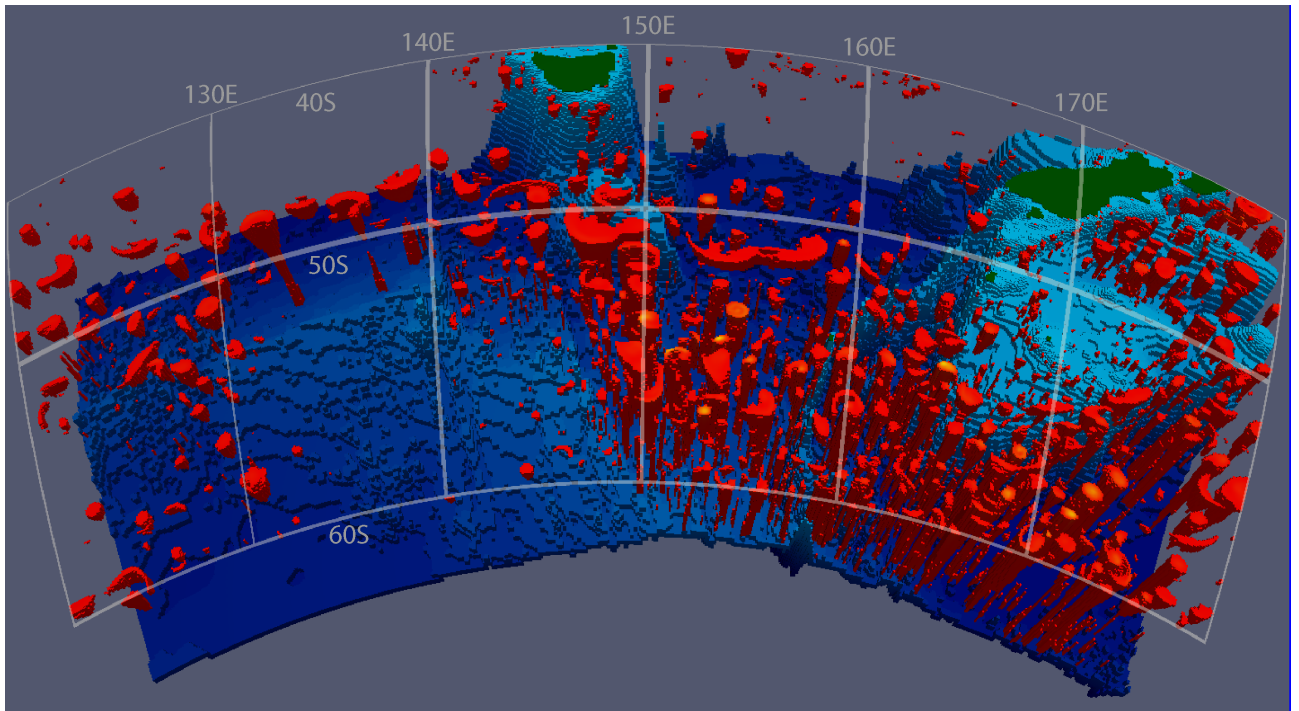


Figure 1. Okubo-Weiss field in the Southern Ocean to the south of Tasmania and New Zealand, showing 120°E – 180°E and 45°S – 55°S and an isosurface of $W/\sigma_W = -0.2$. The Antarctic Circumpolar Current is the region with the largest number of eddies and the deepest eddies in the world. Many of these eddies extend to the full depth of the ocean; others are strictly surface features, and some are completely submerged. The R^2 method is more discriminating, and will eliminate many of the more spurious features seen here. Depth is exaggerated by a factor of 50.

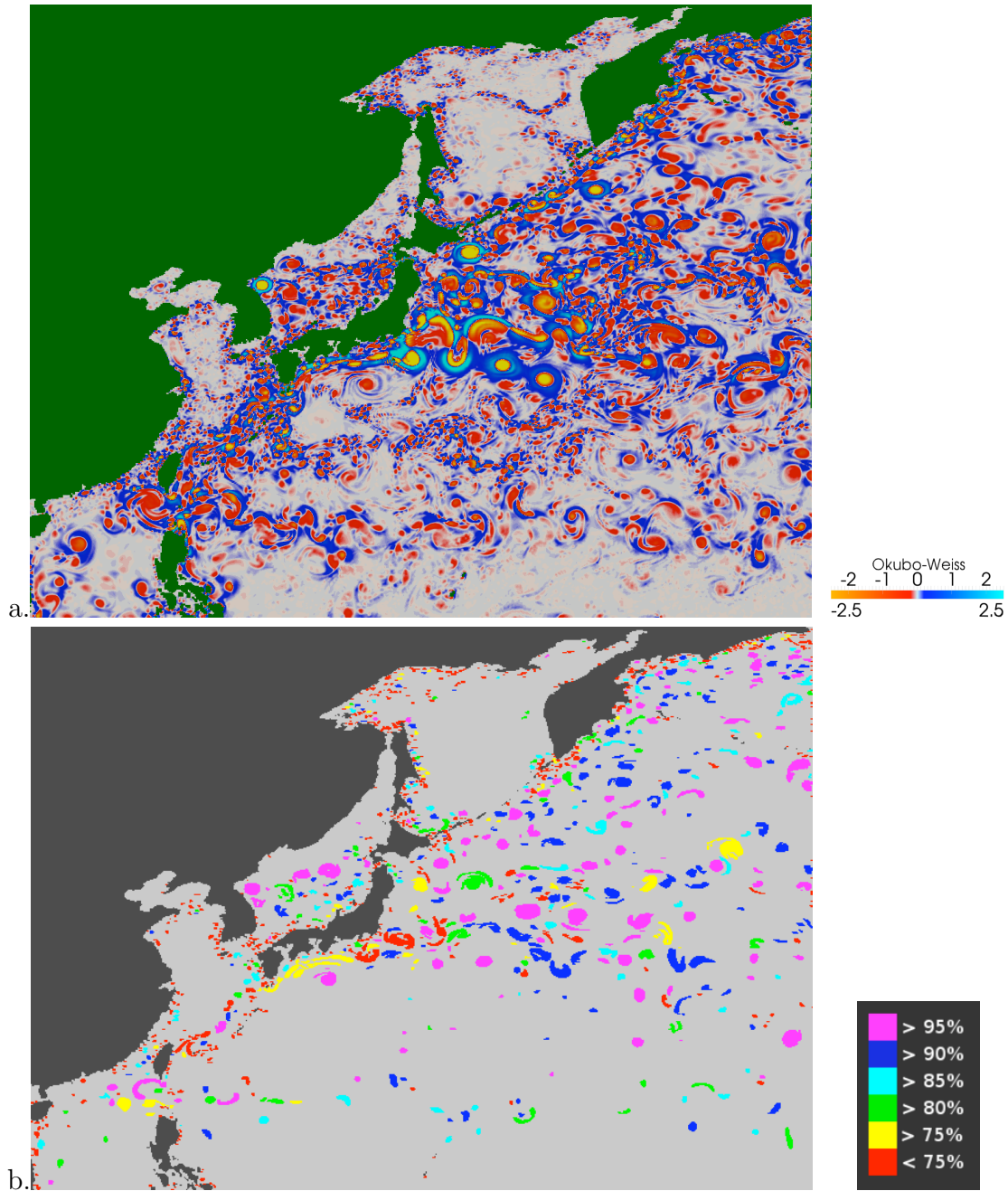


Figure 2. (a) Okubo-Weiss values over a region including the Kuroshio Current. With a standard OW method, all the red areas would be identified as candidate vortices. (b) Using the R^2 method, each high-vorticity feature has a confidence threshold associated with it. Features with a confidence threshold $> 95\%$ (magenta) are well-formed vortices, while those with a confidence threshold $< 75\%$ (red) are small, noisy features, mostly found near land boundaries. Those in between are a mix of sheared and deformed vortices. A 90% confidence threshold is used for the remainder of this study.

D R A F T

March 6, 2013, 10:41am

D R A F T

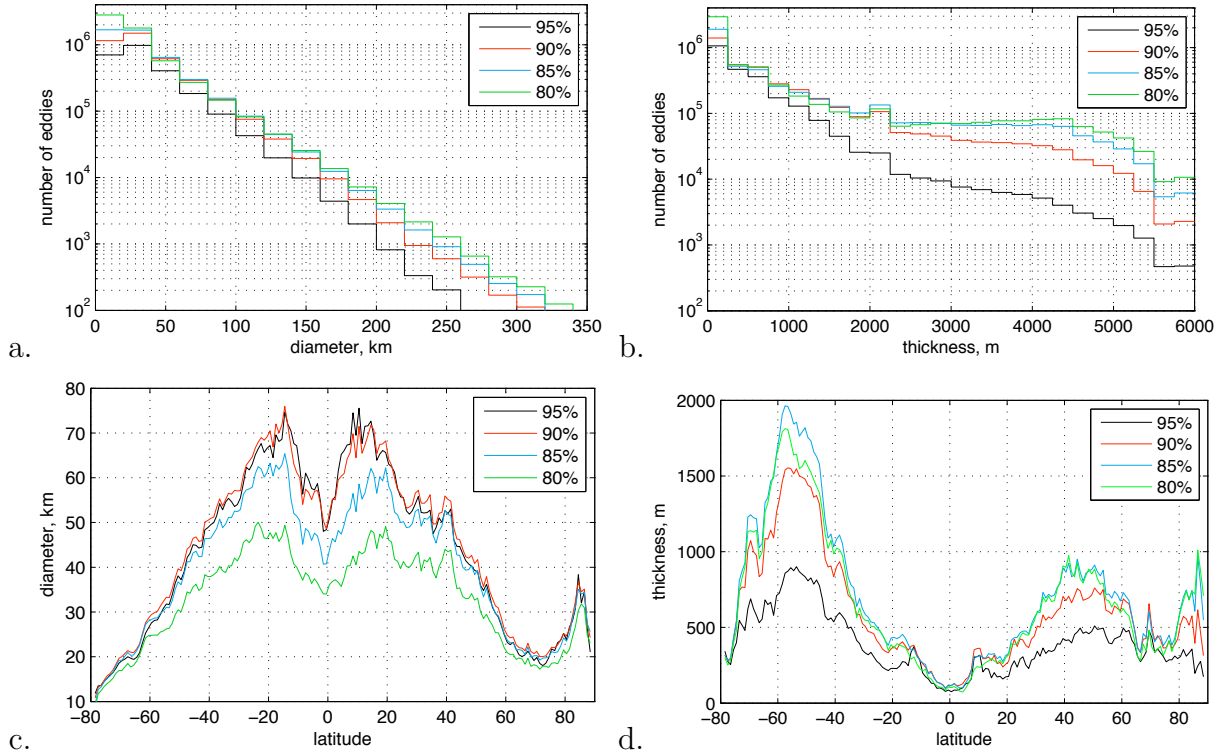


Figure 3. Sensitivity analysis where the confidence threshold of the R^2 method has been varied between 80 and 95%, showing a distribution of (a) eddy diameter; (b) thickness; (c) mean diameter versus latitude; and (d) mean thickness versus latitude. As the confidence threshold is increased, the algorithm becomes more selective in accepting eddies. The majority of eddies removed are less than 20km in diameter, making mean diameters larger. Both thin and thick eddies are removed as the confidence threshold increases, so that mean eddy thickness is a maximum at the 85% confidence threshold. The sensitivity analysis was conducted on one year’s daily data, with no minimum eddy lifetime.

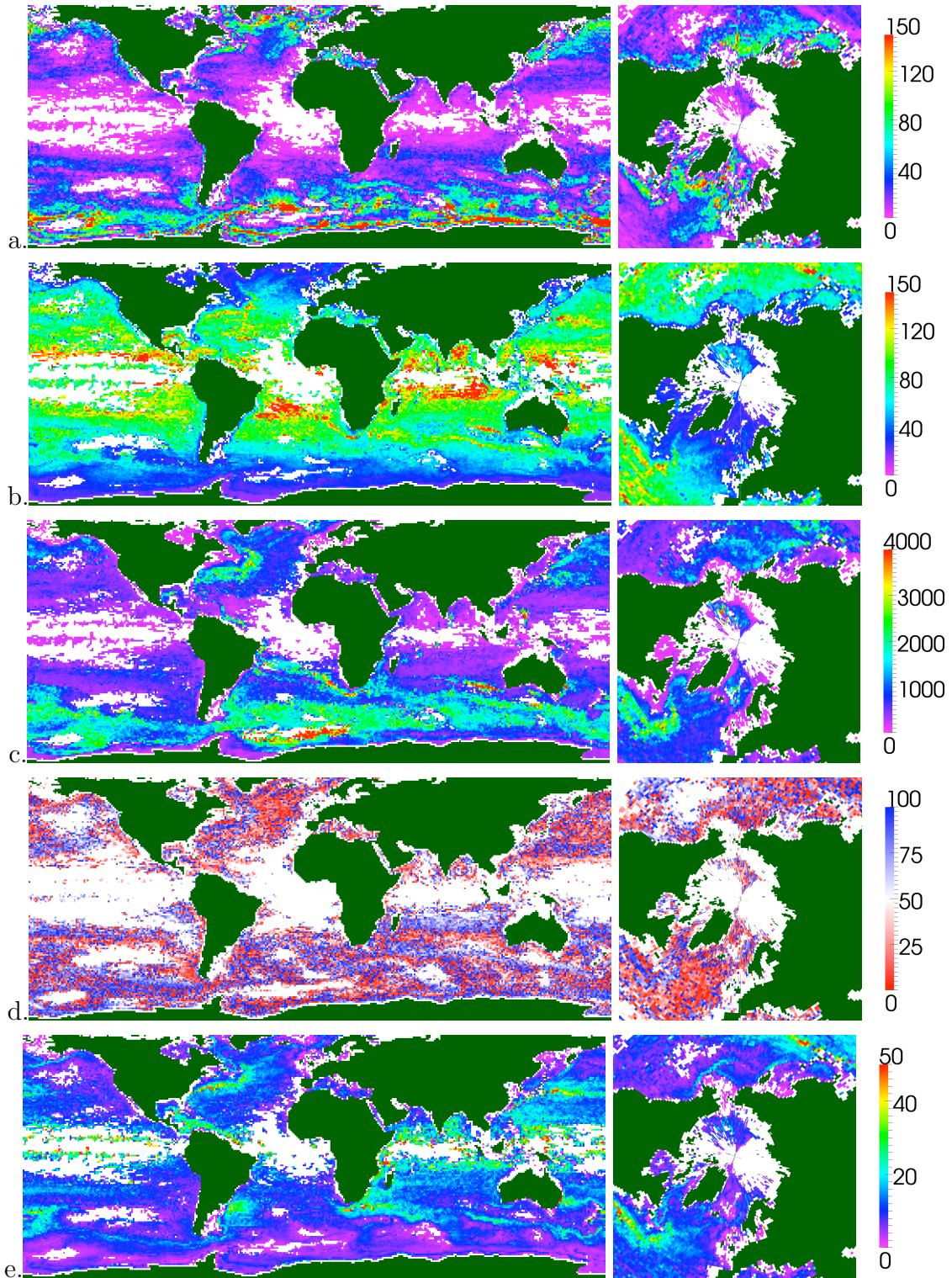


Figure 4. Eddy statistics from seven years of a POP ocean simulation using the R^2 eddy detection method, a minimum lifetime of four weeks, and collated in 1° bins: (a) daily eddy count, where color scale is eddies per year; (b) diameter, km; (c) thickness, m; (d) percent cyclonic; and (e) eddy propagation speed, cm/s. White areas are 1° cells where no eddies were detected over the seven year census.

D R A F T

March 6, 2013, 10:41am

D R A F T

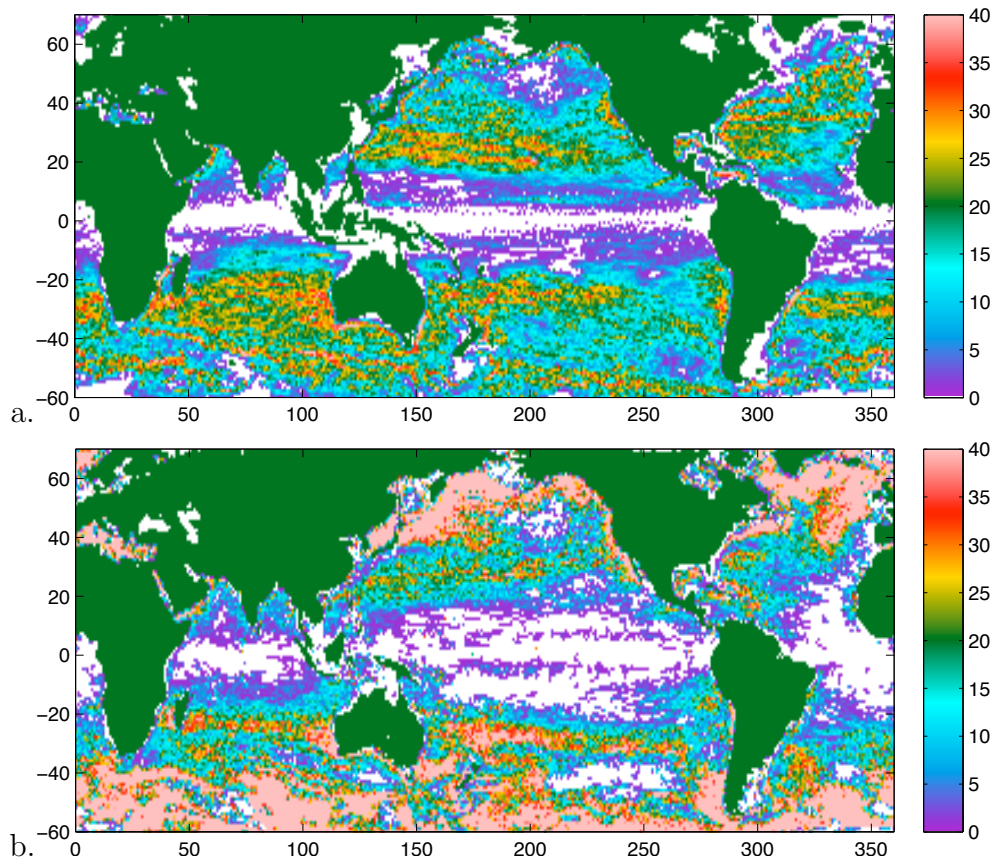


Figure 5. Number of eddies per one degree square from (a) satellite observations of *Chelton et al.* [2011] and (b) this study. Color bar extents were chosen to compare geographical distribution rather than magnitude, as there are several differences between data sets (see text). Overall, observations show a higher eddy density in zonal mid-basin bands, while the simulations produce more eddies in western boundary currents and the ACC.

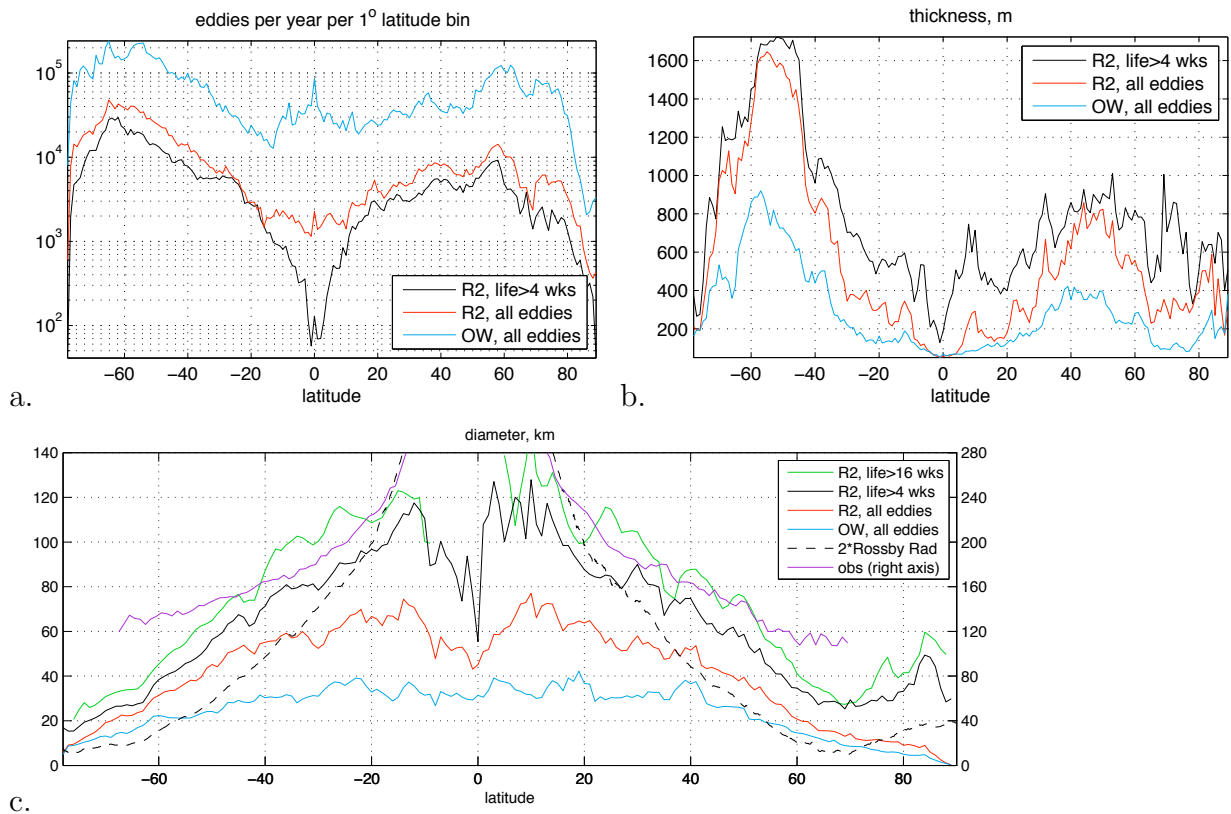


Figure 6. Eddy statistics collected over a seven year ocean simulation in 1° latitude bins: (a) daily eddy count; (b) thickness; and (c) diameter, showing the Okubo-Weiss method (blue), the R^2 method (red), and the R^2 method with a minimum lifetime of four weeks (black) and 16 weeks (green, c only). The black dashed line in (c) is two times the first baroclinic Rossby Radius computed using the time-averaged model density field employing the method described in Section 2a of *Smith et al.* [2000]. Note that this curve is almost identical to that produced from the model’s data-derived initial condition. The purple line in (c) shows the zonally averaged speed-based radius scale from *Chelton et al.* [2011] (note scale is on right axis). The R^2 method is more selective than Okubo-Weiss alone, and the lifetime filter further reduces the number, particularly near the equator. Eddies rejected by the R^2 method tend to be small and thin, so that the average eddy diameter and thickness increase. Eddy numbers are counted from each daily entry of the census data.

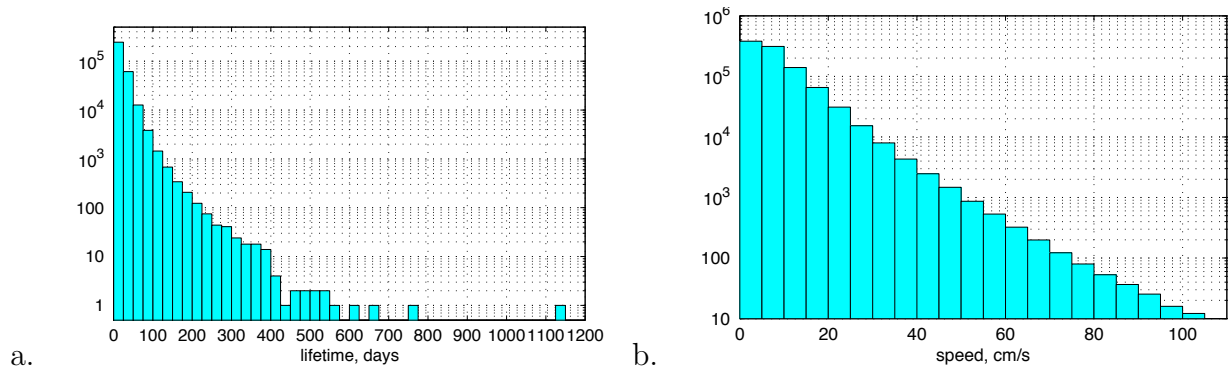


Figure 7. Distribution of eddies detected by (a) lifetime and (b) propagation speed, using the R^2 method. The majority of eddies are relatively slow and short-lived, but some eddies exist for more than a year. In (a) the vertical axis shows the eddy count for all seven years, and each eddy is only counted once over its lifetime. In (b) the vertical axis shows number of eddies per year counted in each daily snapshot. Eddies in (b) have a minimum lifetime of four weeks.

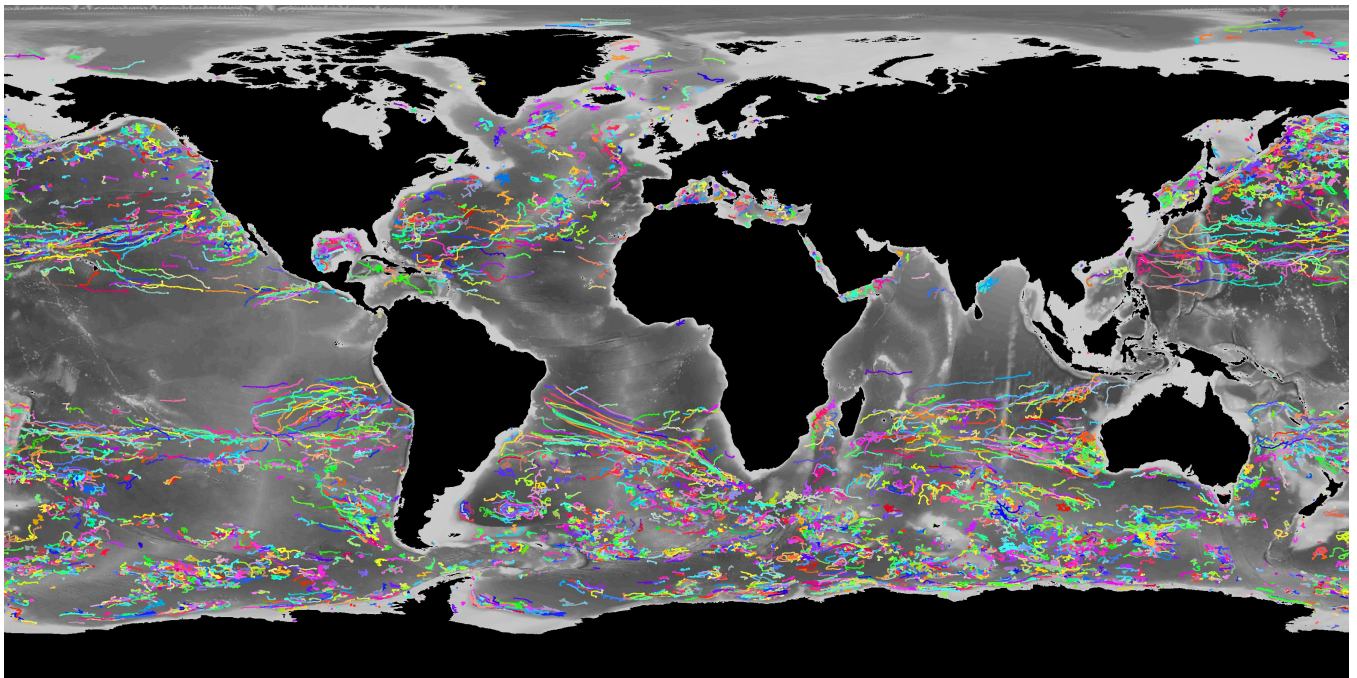


Figure 8. Tracks trace each eddy over its lifetime for the 5000 longest-lived eddies over the seven-year simulation overlaid on a grayscale bathymetry map. Colors are randomly assigned to identify each eddy track.

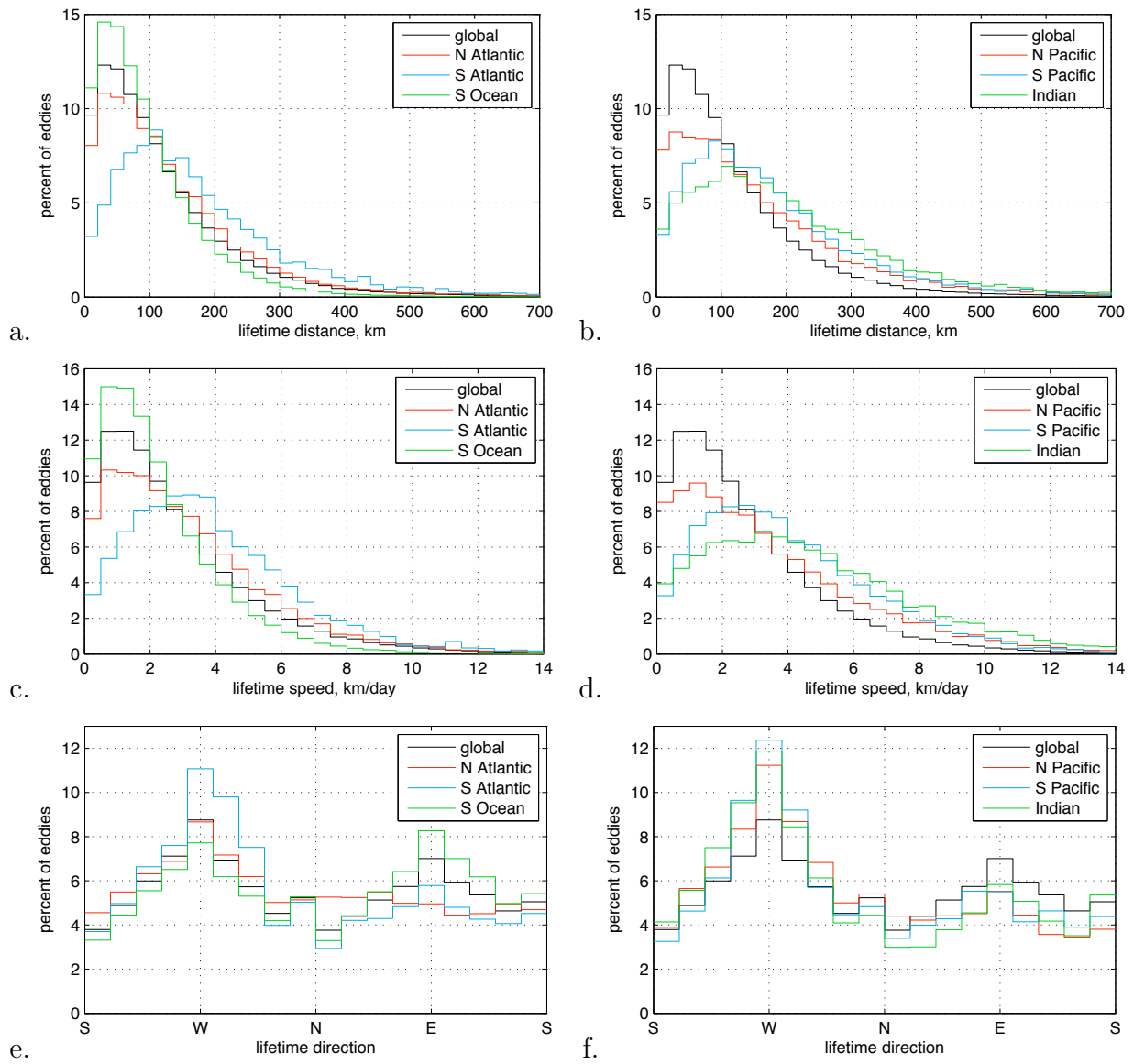


Figure 9. Statistics averaged over the lifetime of an eddy: distance (a,b); speed (c,d); and direction (e,f), shown for various regions. Only eddies with a minimum lifetime of 28 days are considered.

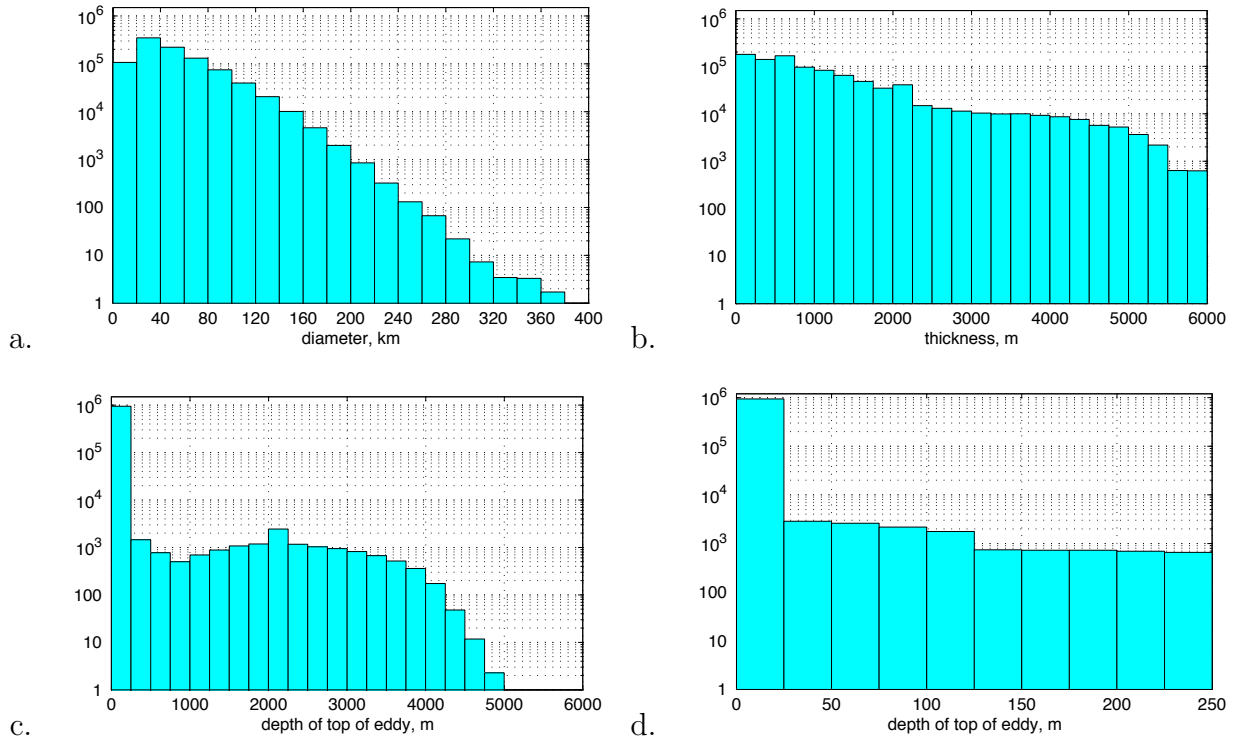


Figure 10. Distribution of eddies detected by (a) diameter; (b) thickness; and (c,d) depth of the top of the eddy, using the R^2 method and minimum lifetime of four weeks. The last plot (d) shows detail of the first bar in (c). Data includes the population of eddies recorded each day for seven years, and vertical axes display the number of eddies per year. The majority of eddies are small and thin, but there are still thousands of eddies with diameters greater than 200km, and tens of thousands with thicknesses of 4000-5000m. The great majority extend to the surface (c), but tens of thousands exist below the surface.

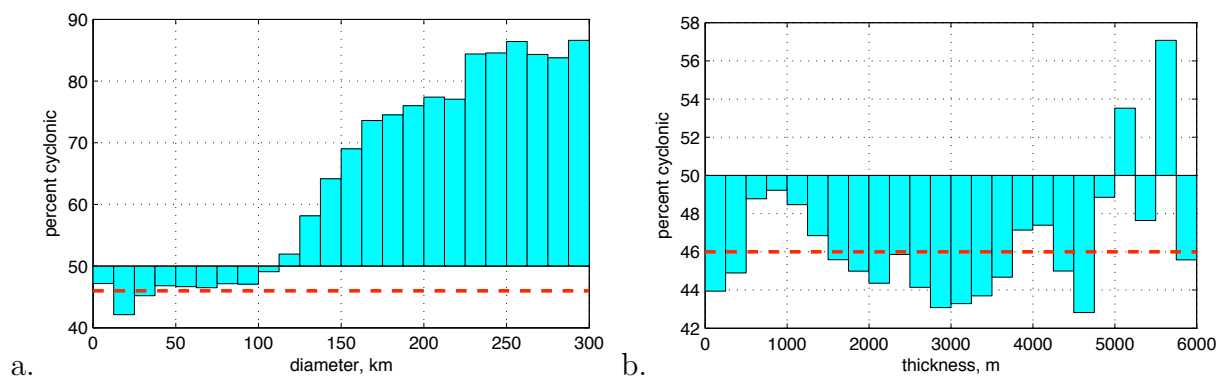


Figure 11. Percent of eddies that are cyclonic, binned by diameter (a) and thickness (b). Overall, 46% of eddies are cyclonic (dashed line). A strong correlation exists between cyclonicity and eddy diameter, and there appears to be little dependence on thickness.

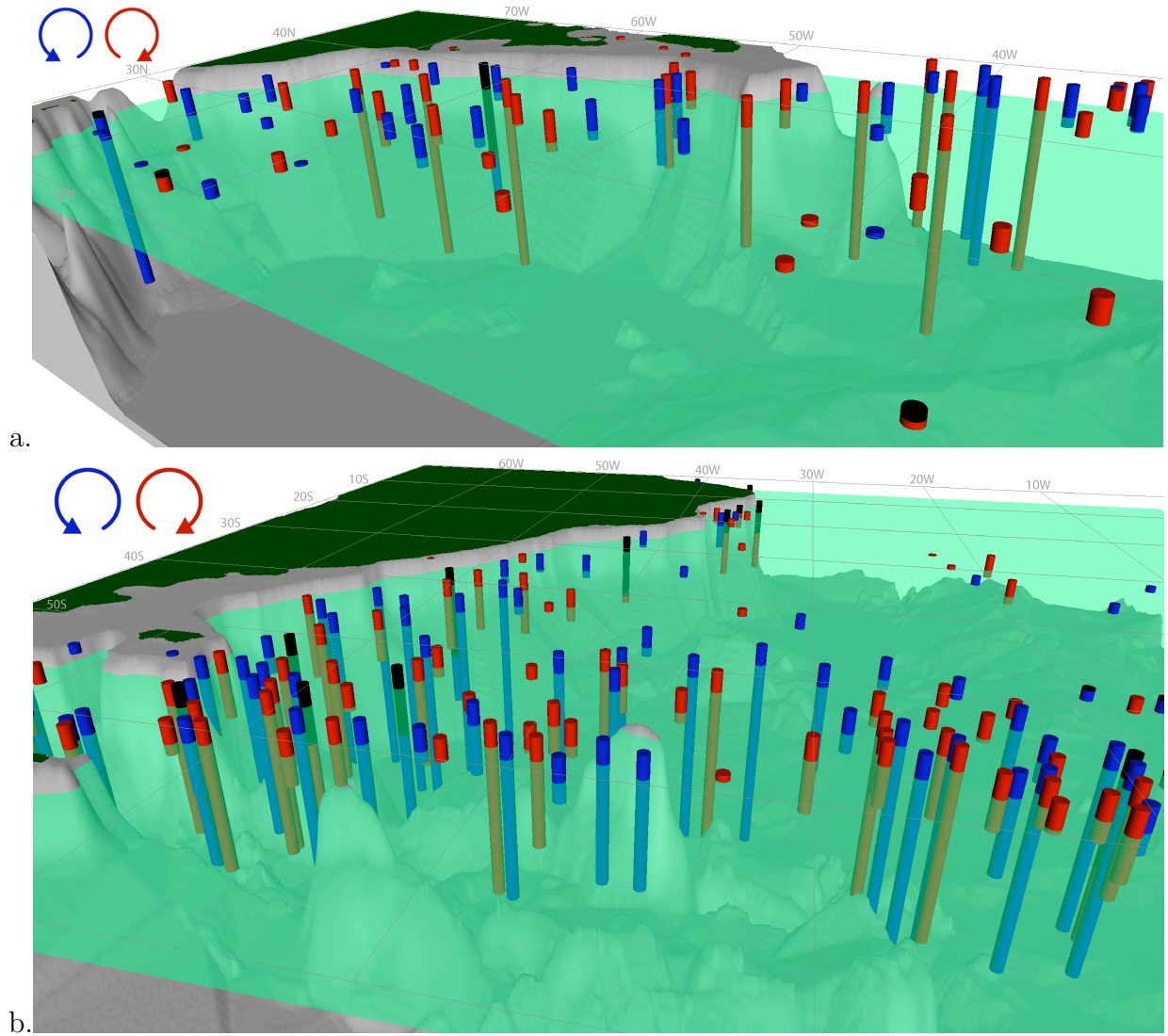


Figure 12. Skeletonized view of eddies in (a) the North Atlantic and (b) the South Atlantic. The translucent green planes are at 700m (a) and 500m (b). These images show the depth of penetration of the eddies; most extend to the bottom in the Antarctic Circumpolar Current region, while less than half of the Gulf Stream eddies penetrate deeply. Eddies with positive vorticity are red above the planes and yellow below; eddies with negative vorticity are blue above the planes and cyan below. Black columns extend the subsurface eddies to the surface to aid visualization. Depth is exaggerated by a factor of 50. (Image from Fig. 4 and 5 of *Williams et al.* [2011a])

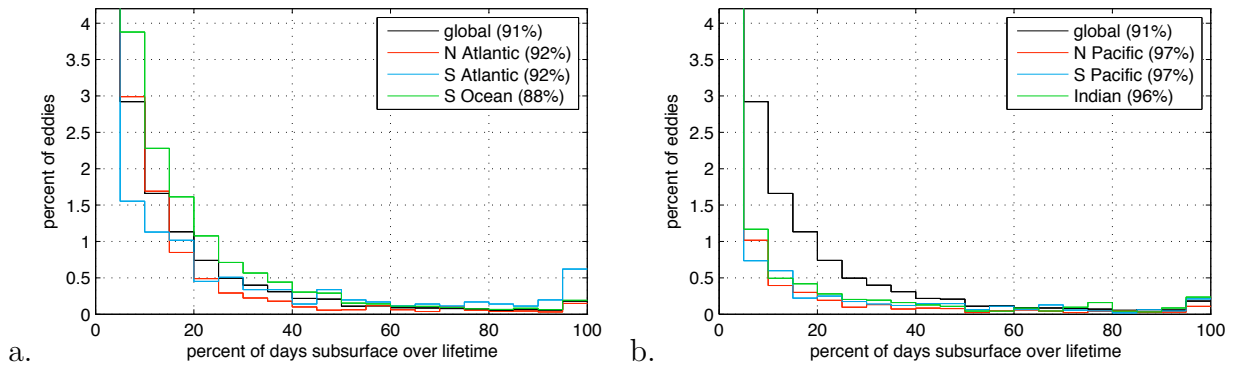


Figure 13. Distribution showing percent of days eddies are subsurface over their lifetime for various regions, for eddies with lifetimes of at least 28 days. Here subsurface means the top surface of the detected eddy is below 100m. Parenthesis on the legends show the value of the 0–5% bin so that the vertical scale can show the detail of the other categories. The values in the legend show that the great majority of eddies are subsurface for 5% of the time or less; i.e. eddies nearly always extend to the surface.

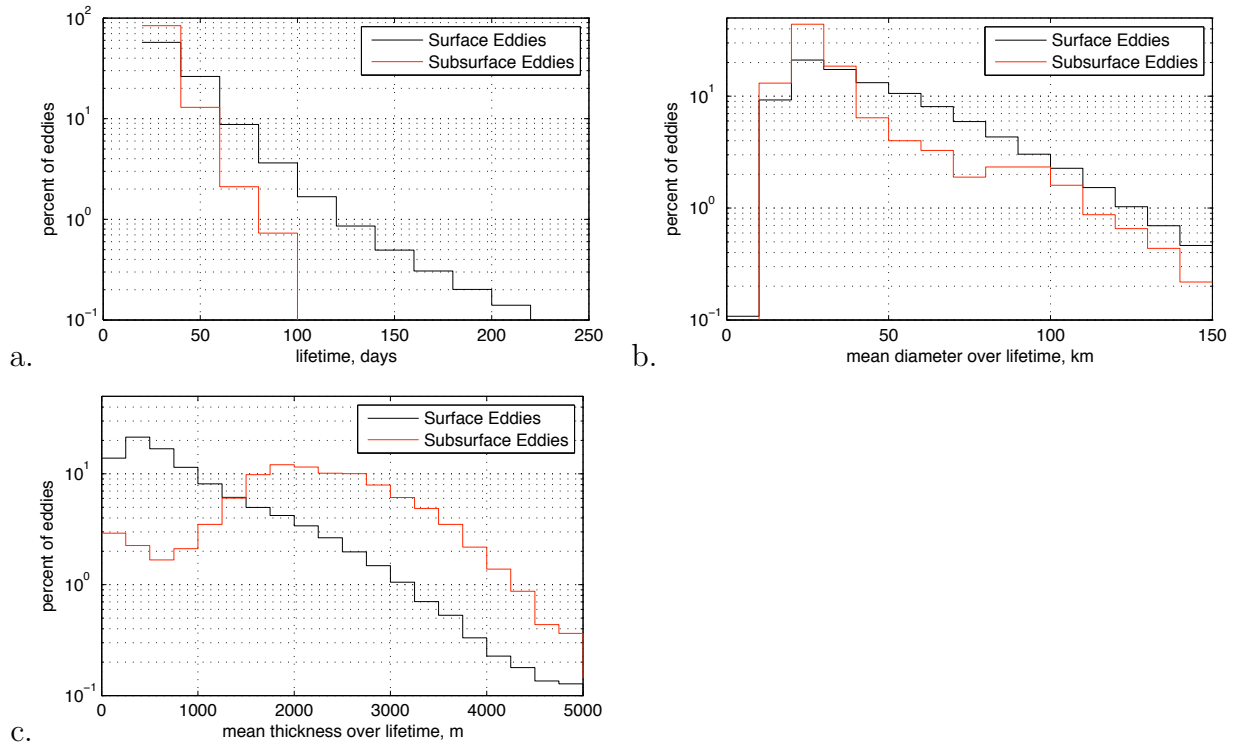


Figure 14. Characteristics of surface versus subsurface eddies, for eddies with lifetimes of at least 28 days. Subsurface eddies are defined as those below 100m at least 50% of their lifetime, and surface eddies are below 100m 5% of their lifetime or less. Subsurface eddies have a shorter lifetime (a) and smaller diameter (b) than surface eddies. Subsurface eddies have a larger percentage of eddies thicker than 1500m than surface eddies (c). Overall, most eddies are thin surface eddies that only extend 500-1000m below the surface (c).

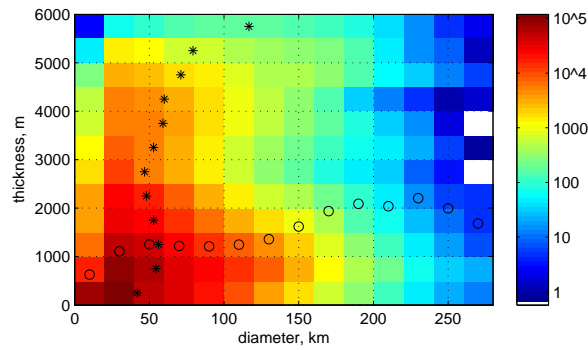


Figure 15. Distribution of eddies binned by diameter versus thickness using R^2 method and minimum lifetime of four weeks. Colors show a log scale of number of eddies recorded daily, per year. For each thickness category, the mean diameter is starred; for each diameter category, mean thickness is circled. A weak correlation is seen—thick eddies tend to be larger in diameter than thin eddies.

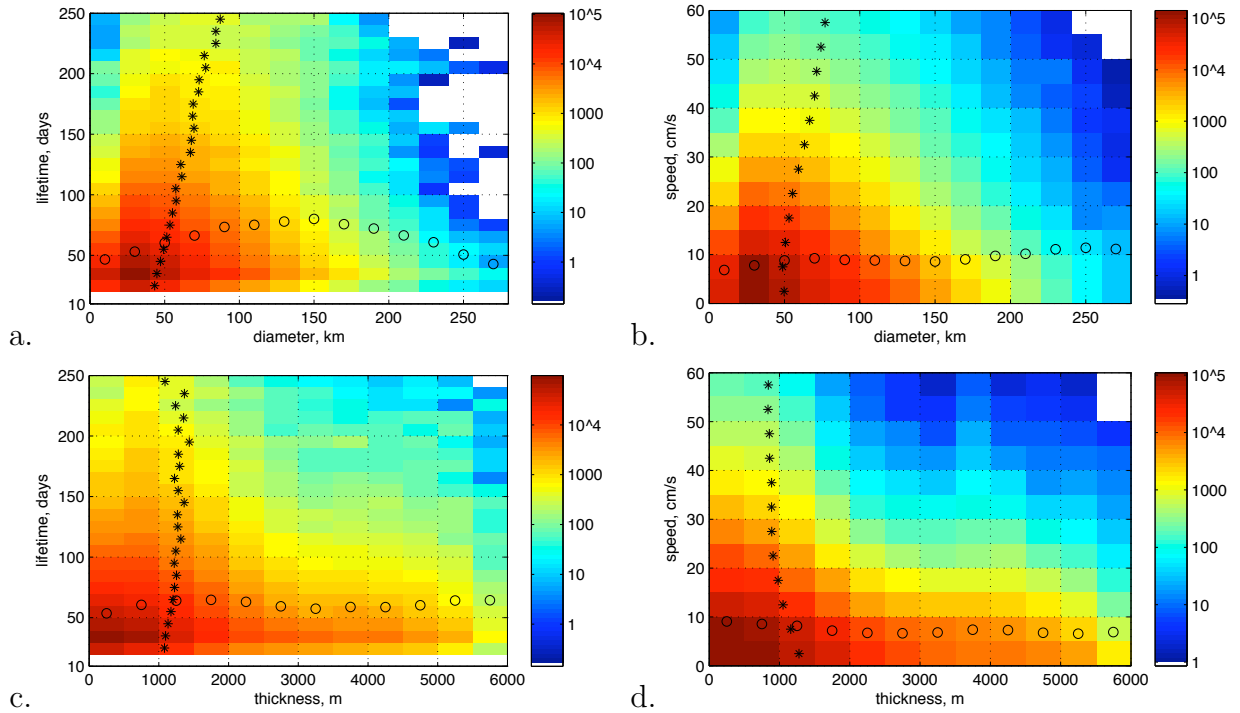


Figure 16. Distribution of eddies binned by lifetime (a,c) and propagation speed (b,d) versus diameter (a,b); thickness (c,d), all using R^2 method and minimum lifetime of four weeks. For each category, an asterisk is placed at the average of the horizontal variable, and a circle at the average of the vertical variable. White areas contain no data. Colors show a log scale of number of eddies recorded daily, per year. These trends show that longer-lived and faster eddies tend to be larger in diameter (a,b), and very thin eddies are shorter-lived and faster (c,d).